Revealing the nature of glass by the hyperquenching-annealing-calorimetry approach

Yue, Yuanzheng

Published in:
Journal of Non-Crystalline Solids: X

DOI (link to publication from Publisher):
10.1016/j.nocx.2022.100099

Publication date:
2022

Document Version
Publisher's PDF, also known as Version of record

14 (2022) 100099

Contents lists available at ScienceDirect

Journal of Non-Crystalline Solids: X

journal homepage: www.sciencedirect.com/journal/journal-of-non-crystalline-solids-x

Revealing the nature of glass by the hyperquenching-annealing-calorimetry approach

Yuanzheng Yue *

Department of Chemistry and Bioscience, Aalborg University, DK-9220 Aalborg, Denmark

ARTICLE INFO

Keywords:
Glass
Hyperquenching
Sub-T_g annealing
Calorimetry
Energy bird
Structural heterogeneity
Shadow glass transition
Fragile-to-strong transition

ABSTRACT

C. Austen Angell has been a great inspiration for liquid and glass scientists including myself. He was a close collaborator of mine on glass dynamics and thermodynamics, particularly on the sub-T_g relaxation in glass. Here, in memory of his seminal contributions to science and our collaboration, I revisit our published data and analyze our unpublished data, as well as review some of important results reported recently in the literature, concerning the sub-T_g relaxation in glass, a field on which Austen has profoundly impacted. I highlight new insights into the dynamics, thermodynamics, and structural heterogeneity in glass far from equilibrium, based on the hyperquenching-annealing-calorimetry (HAC) experiments. I describe key extensions and applications of the HAC approach in glass research. Finally, I present the perspectives and challenges regarding the sub-T_g relaxation in glasses with fictive temperatures well above T_g.

1. Introduction

Austen Angell was a visionary researcher who made a paradigm shift in the science of liquids and glasses, yet he was also a modest scholar who always encouraged and advised other scientists to conduct their own original research. In his academic career, he was in pursuit of an overarching big picture of the nature of glass and liquids, and he made substantial progress towards this goal [1–4]. One of his major research fields was the glass transition and glass relaxation. His passion, curiosity, and vision for this complicated but fascinating field has deeply impacted the research of many scientists, including myself.

One of the research fields that Austen has significantly influenced is the glass transition and relaxation. In this article, I focus on the current understanding of sub-T_g relaxation in glass, to which Austen had also greatly contributed. Studying the sub-T_g relaxation has become a powerful approach to reveal the dynamic and thermodynamic nature of glass and glass transitions. It is also inspiring that Austin made significant progress in investigating the sub-T_g relaxation over the past decades. However, many challenges remain in the study of sub-T_g relaxations. One of the main challenges is the lack of direct experimental tools that can capture the structural response to the enthalpy relaxation in glass. In other words, the current characterization techniques are still not sensitive enough to probe glass structure evolution accompanied by relaxation. To overcome these challenges, scientists have been trying to use different ways to monitor the structural evolution in glass during enthalpy relaxation. One effective way is to pose extreme glass forming conditions, e.g., hyperquenching [5–9], high pressure [10–13], tension [14–17] and shearing [18], by which highly excited configurational states and structural change can be arrested in glass [19–23]. Subsequently, the excited glass is partially annealed via dynamic or isothermal heating below the glass transition temperature (T_g), and afterwards undergoes reheating in a differential scanning calorimeter (DSC) and various characterizations. Through this research strategy, we have observed many fascinating features of the enthalpy relaxation in the annealed rapidly quenched glass below T_g (i.e., the so-called sub-T_g relaxation), which cannot be detected by other means. Over the past two decades, my research group has been investigating the sub-T_g relaxation behavior and physical properties of various families of melt-quenched glasses such as oxides, chalcogenides, alloys, and metal-organic frameworks (MOFs), most of which are subjected to hyperquenching or compression or tension during glass formation. The other effective way is to perform the atomistic modeling on glasses and glass-forming liquids under extreme glass-forming conditions. The modeling approach exhibits promising perspectives, especially owing to the continuing advances both in enhancing the computing capability and in developing glass theories. This article focuses on reviewing the experimental studies on the sub-T_g relaxation in hyperquenched glasses, which have provided insights into the nature of glass and glass transition [9,19–23].

* Corresponding author.
E-mail address: yy@bio.aau.dk.

https://doi.org/10.1016/j.nocx.2022.100099
Received 11 February 2022; Received in revised form 10 April 2022; Accepted 11 April 2022
Available online 14 April 2022

In 1999, I started to develop the calorimetric approaches and concepts for studying sub-T_g relaxation in stone wool glass fibers formed at the cooling rate of $>10^6$ K s^{-1} in collaboration with Rockwool International. In 2001, I presented a poster that reflected my findings concerning the sub-T_g enthalpy relaxation at the 4th International Discussion Meeting on Relaxations in Complex Systems (4th IDMRCS) in Creta, Greece, in 2001. It was fortunate for me that Angell noticed my poster and expressed strong interest in my findings. He had a long chat with me and gave insightful advice regarding how to connect my results with the potential energy landscape (PEL) of glass-forming liquids and the glass transition in water and other glass formers. At this conference, he called our extremely fast cooled stone wool fibers "hyperquenched (HQ)" glass. At the time, although I had known Austen's name for long time through several of his seminal papers, the first time I met him in person was at the 4th IDMRCS. Inspiringly, after the conference he sent me a very long e-mail, in which he wrote: "…It was very nice to meet you at this meeting in Creta, and to learn of the nice measurements you have been making. I hope that people will be aware of the significance of your results….". I was very impressed by his enthusiasm, curiosity and insight for scientific problems. Since then, we had been collaborating and communicating with each other, and as a reward we published four joint papers [9,20,24,25]. The last time I met him was at the Angell International Symposium on Molten Salt, Ionic and Glass-forming Liquids held in Cyprus, in October 2019 in celebration of his scientific contributions. I was honored to co-chair the symposium and had exciting discussions with him.

This article portrays the role of my collaboration with Austen in studying the sub-T_g relaxation in the HQ glass systems. It describes our present understanding of the enthalpy relaxation behavior in the glass far from equilibrium, i.e., the glass that forms under extreme conditions. I present several key findings that we achieved using the HQ-annealing-calorimetry approach. I briefly discuss the applications of the approach in understanding other fundamental glass problems, as well as in improving glass production technology. This article is based on both the published and unpublished data, i.e., it is a combination of a review article and an original article. I should mention that a recent comprehensive review describes the current understanding of glass through differential scanning calorimetry [23]. In contrast, the present article describes the advances in studying the sub-T_g glass relaxation, which were achieved using the hyperquenching-annealing-calorimetry approach that we established [8,9,19,20,24–27]. These advances are closely associated with Austen's contributions and inspirations. In addition, the present article gives new insights into the sub-T_g relaxation and structural heterogeneity, which are crucial in revealing the nature of glass.

2. Experimental section

2.1. Sample preparation and collection

The stone wool fiber samples involved in this article has the chemical composition (mol%): 47.5SiO_2, 9.1Al_2O_3, 6.6FeO, 15.9CaO, 16.9MgO, 2.0Na_2O, 0.7K_2O [28]. The origin of the name 'stone wool' is related to its raw material such as basalt stone and other minerals. The stone wool fibers were spun from a homogenized melt using the cascade centrifugal process (see the upper left panel in Fig. 1) [28]. The rotation of the spinning wheels leads to formation of stone wool fibers with a mean diameter of 3–5 μm and a mean length of up to 5 mm. Under the above conditions, the fibers were quenched at up to ~10^6 K s^{-1} [28], and thus this process is referred to as hyperquenching [8].

The glass wool fibers with the composition (mol%) of xCaO-(100-x) SiO_2, where x = 34, 40, 55, were produced under the same spinning condition as that for stone wool fibers [29]. The silica glass fibers were produced using the preform approach [30]. The silica fiber samples contain 100 ppm hydroxyl groups. The diameter of the fibers is around 10 μm.

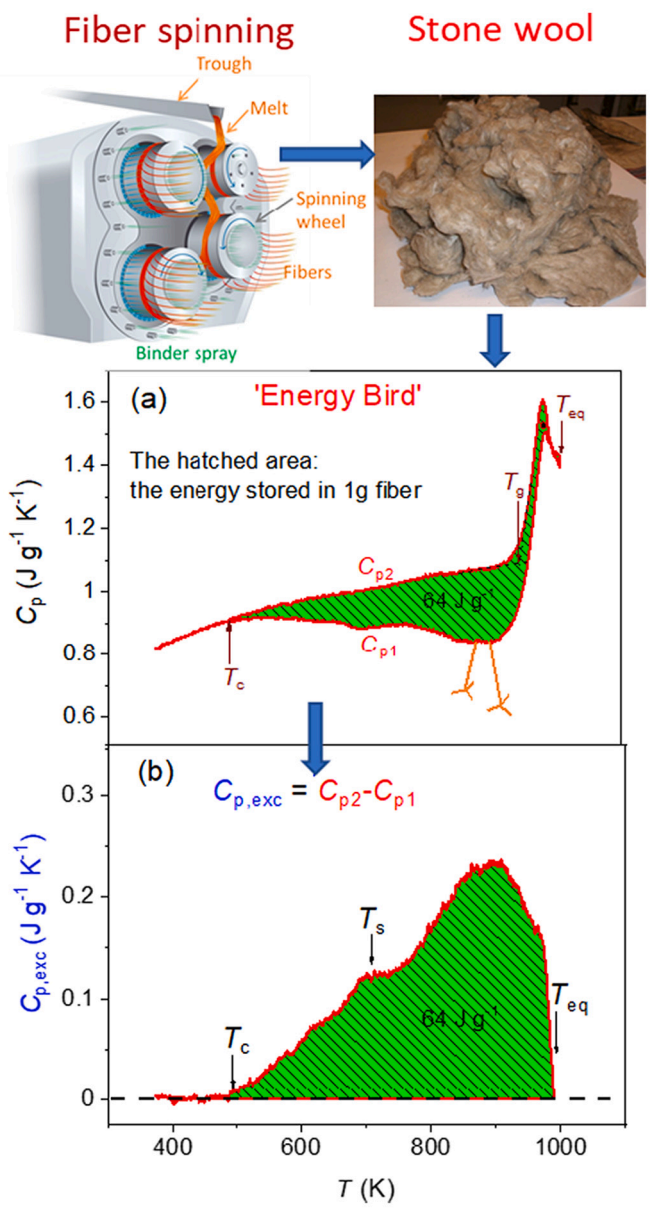

Fig. 1. The 'energy bird' approach for the sub-T_g enthalpy relaxation. Upper left panel: Fabrication process of stone wool [28], which is a hyperquenching process (cooling rate: ~10^6 K s^{-1}) [26]. Upper right panel: The produced stone wool. **(a)** Isobaric heat capacities (C_{p1} and C_{p2}) of stone wool against temperature (T), measured during the first and second DSC upscans at 0.333 K s^{-1}, respectively. This C_p pattern is here called "energy bird", which describes the excessive energy (see the hatched area) stored in HQ sample relative to the sample cooled at the standard rate of 0167 K s^{-1}. T_c: onset temperature of the enthalpy release; T_g: glass transition temperature (941 K); T_{eq}: Equilibrium temperature (1005 K), which is the offset temperature of the energy release peak at $C_{p2} = C_{p1}$. **(b)** The released enthalpy per Kelvin ($C_{p,exc} = C_{p2} - C_{p1}$) versus T. T_s: the 'shoulder' temperature, implying a partial overlap of two energy release peaks. Reproduced with permission from Ref. 8.

The volcanic glass fibers were collected from Hawaii Island, which are often called Pele's hair since it looks like hair. Pele's hair formed when molten lava is thrown into the air during explosive eruptions, stretched and rapidly quenched. These hair-like fibers are about 100 to 200 μm in diameter, and 1 to 3 cm in length. Their chemical composition is a typical basaltic composition that can be found in [31,32]. Pele is said to be the 'Hawaiian goddess' of volcanoes and to be harsh on people who take stones from her domain.

The apatite glass (a kind of bioglass) involved in this work has the chemical composition (wt%): 22.5SiO_2, 20.1Al_2O_3, 18.1CaO, 22.8P_2O_5, 9.2K_2O and 7.3F. Some apatite glass samples were obtained by melting the raw materials in an alumina crucible at 1773 K, and then remelting the crushed glass frits in Pt crucibles at 1773 K and finally casting the melts onto a graphite mold. The thus-cooled glass is here referred to as 'slowly quenched glass'. Some apatite glass samples were produced by the above-mentioned melting procedure, and then by pressing the derived melt into a thin glass sheet by a copper block to enhance the cooling rate. The thus-cooled glass is referred to as 'rapidly quenched glass'. Note that many tiny fluorapatites crystals are already present in the as-produced glass since the glass system has strong tendency to crystallization, i.e., low glass forming ability [33].

The metal-organic framework (MOF) glass, ZIF-62 (Zn$(Im)_{1.75}(bIm)_{0.25}$] (Im: imidazolate; bIm: benzimidazolate) was prepared by melting its counterpart crystal and subsequently quenching the melt at 0.167 K s^{-1}. ZIF-62 crystals were synthesized using a solvothermal method described in [34].

The glass with the composition (wt%): 74SiO_2-16Na_2O-4CaO-6FeO (i.e., SNCF glass), where 32% of iron was enriched in the resonant ^{57}Fe isotope, was prepared to investigate the impact of both hyperquenching and annealing on the vibrational density of states (VDOS) of glass [35]. The SNCF glass was produced by dropping its corresponding melt film (about 100–200 μm in thickness) into water, giving a cooling rate of about 10^3 K s^{-1}. The annealed sample was obtained by annealing the quenched thin film at 785 K for 30 min and then by cooling them at 3×10^{-2} K s^{-1}. The Mössbauer spectroscopy indicated tetrahedral coordination of iron to oxygen, implying that iron substitutes for silicon in the network structure [35].

A series of metallic glasses were prepared by arc-melting the ingots with the composition of $(Cu_{50}Zr_{50})_{100-x}Al_x$ (x = 0, 2, 4, 8) (in atom%) in argon and subsequently quenching the resulting melt using single copper-roller spinning. This series of hyperquenched glasses was used to study the thermodynamic and structural sources of the fragile-to-strong (F-S) transition in metallic glass-forming liquids by using a combined approach of the viscometry-calorimetry-X ray scattering [22].

2.2. Sub-T_g annealing, calorimetry and viscometry

The hyperquenched (HQ) glass samples, such as stone wool, Pele's hair, CaO-SiO_2 glasses, apatite glasses, SNCF glass, MOF glasses and metallic glasses, were annealed in argon at various temperatures (T_a) below T_g for different durations (t_a) prior to calorimetric scans. Argon was used as the purge gas to prevent redox reaction during annealing. In contrast, HQ CaO-SiO_2 glasses and HQ vitreous silica were annealed in air atmosphere. The apatite glasses were not annealed before calorimetric scans.

After annealing, the isobaric heat capacity (C_p) curve of each sample was measured using a differential scanning calorimeter (DSC) (Netzsch STA449C Jupiter). The samples were put into a platinum crucible situated on a sample holder of the DSC at room temperature. The samples were upscanned at 0.333 K s^{-1} to the offset temperature of the glass transition peak, and then cooled back to 473 K at 0.333 K s^{-1}, thus forming the standard glass. After natural cooling to room temperature, the second upscan was conducted using the same procedure as for the first. The MOF glasses and apatite glasses were subjected to only the first DSC upscan. To determine the C_p curve of the samples, both the baseline and the sapphire as reference were measured. The details of the experimental procedures can be found in [19,20,27,36].

To determine the cooling rate of Pele's hair, the viscosity-temperature relationship of its corresponding volcanic melt was determined. The high-viscosity data of the volcanic melt were acquired using a micropenetration viscometer (Baehr DIL 802 V), while the low-viscosity data were obtained by a concentric cylinder viscometer (Physical Rheolab MC1 Paar Physica) [37]. Note that the viscosity-temperature data in the intermediate viscosity range of 10^4–10^7 Pa s were not obtained since the volcanic melt has strong tendency to crystallize in this range.

2.3. Determination of vibrational dynamics and structure in HQ glasses

To investigate the impact of sub-T_g annealing on vibrational dynamics of HQ stone wool, the cold neutron scattering time-of-flight measurements were carried out using the Disk Chopper Spectrometer at the National Institute of Standards and Technology for Neutron Research. The detailed experimental conditions were given in [9]. The vibrational density of states in SNCF glass was determined using nuclear inelastic scattering at the Nuclear Resonance Beamline ID18 of the European Synchrotron Radiation Facility [35]. The structural evolution in CuZrAl glasses during the F-S transition was probed by performing the X-ray scattering measurements on the Bruker-AXS D8 ADVANCE x-ray diffractometer equipped with a diffracted beam monochromator set for a Cu Kα radiation [22].

3. Relaxation in hyperquenched glasses

3.1. 'Energy bird'

In 1999, we started to investigate the thermal and rheological behaviors of stone wool (typical heat insulator and fire barrier) in collaboration with Rockwool International A/S. The users of stone wool products know that the stone wool is made from stones (such as basalt and other minerals) produced by the cascade spinning process (see the upper panel in Fig. 1). However, most of them did not expect it to be glassy. When I conducted the first calorimetric measurements on stone wool, I was really attracted by the fascinating DSC curves, i.e., the sub-T_g enthalpy relaxation pattern as shown in Fig. 1a, where the C_{p1} curve of the fresh wool sample is plotted together with the C_{p2} curve of the 'standard' sample cooled at 0.167 K s^{-1} (10 K/min). The C_{p1} and C_{p2} curves were obtained during the first and the second DSC upscans, respectively. From the relaxation patterns, it was found that stone wool is 'very glassy', since it stores significantly larger enthalpy compared to the standard sample. This stored large enthalpy implies that the stone wool fibers were quenched at an ultrafast rate that was later found to be ~10^6 K s^{-1}, i.e., they were hyperquenched (HQ). This amount of stored enthalpy should be nearly equal to the potential energy since the mechanical work (pressure times volume change) is so small for the condensed matter that is negligible. For simplicity, the sub-T_g enthalpy relaxation pattern is here called 'energy bird', since it looks like a bird (Fig. 1a). The corresponding experimental approach based on 'energy bird' is here called the 'energy bird' approach. By subtracting C_{p1} from C_{p2}, the excessive heat capacity ($C_{p,exc}$) curve can be obtained as exhibited in Fig. 1b. We found the energy trapped in stone wool to be about 64 J g^{-1} by integrating $C_{p,exc}$ over the temperature range from the onset to the offset of the energy release peak. Using this energy and the enthalpy-matching method [8], the fictive temperature (T_f) of the stone wool fibers was found to be 1150 K, i.e., 23% higher than the standard glass transition temperature (T_g) [8]. The fictive temperature definition and determination are described in detail elsewhere [8,23,38–44].

Here it should be mentioned that Yue's group [8] and Angell's group [5] independently established the enthalpy-matching technique to determine T_f of HQ glasses. The profile and size of 'energy bird' for HQ glasses depend on chemical composition [15–18], liquid fragility [40,45], structural heterogeneity [46,47], thermal history [48–50], pressure [11–43,51,52] and tension [14–17]. From the T_f value and the viscosity-temperature relationship, the cooling rate of the studied stone wool was determined to be ~10^6 K s^{-1} [26], and the determination of cooling rate of a fast quenched natural glass fiber sample is described in the next section.

T_c is the onset temperature of the energy release, while T_{eq} is the offset temperature of the glass transition, at which $C_{p1} = C_{p2}$. The asymmetric $C_{p,exc}$ curve with a shoulder at T_s suggests that α relaxation

(represented by the main peak slightly below T_g) and β relaxation (reflected by the $C_{p,exc}$ part below T_s) overlap with each other. The direct link between the sub-T_g enthalpy relaxation to α and β relaxations was examined by studying the sub-T_g relaxation patterns of HQ glasses with different chemical compositions and different fragilities [53–55].

3.2. 'Energy bird' for uncovering the thermal history of glass

As described in [26], the 'energy bird' allows derivation of the thermal history of any glasses including hyperquenched glasses. The thermal history is characterized by the fictive temperature (T_f) and cool rate (q_c). Fig. 2 demonstrates how 'energy bird' was used to determine the thermal history of volcano glass fibers, i.e., Pele's hair. To determine the cooling rate of HQ glass, a three-steps approach was proposed in our previous studies [8,19,20,26]. The first step is to acquire the 'energy bird' of the HQ glass (Figs. 1a and 2a), from which its T_f value is determined by the enthalpy-matching method. The second step is to determine the viscosity (η)-temperature (T) relation for the glass composition in question using viscometry. The third step is to derive the viscosity value at the temperature equal to T_f and to introduce it into the correlation $\log_{10} q_c = K - \log_{10} \eta(T_f)$, where K is a shift factor. The K value was found in our previous work [26] to be 11.35 in a viscosity range spanning seven orders of magnitude. The K value agrees with that (11.3) derived by Scherer [56]. Through the three-steps approach, the T_f value and the corresponding cooling rate of Pele's hair are found to be about 1043 K ($1.11T_g$) (Fig. 2a) and about 2×10^4 K s^{-1} (Fig. 2b), respectively. This indicates that Pele's hair was subjected to hyperquenching during its formation from the magma melt and did not land in a hot zone, i.e., it did not undergo annealing, otherwise the 'energy bird' would not be obtained.

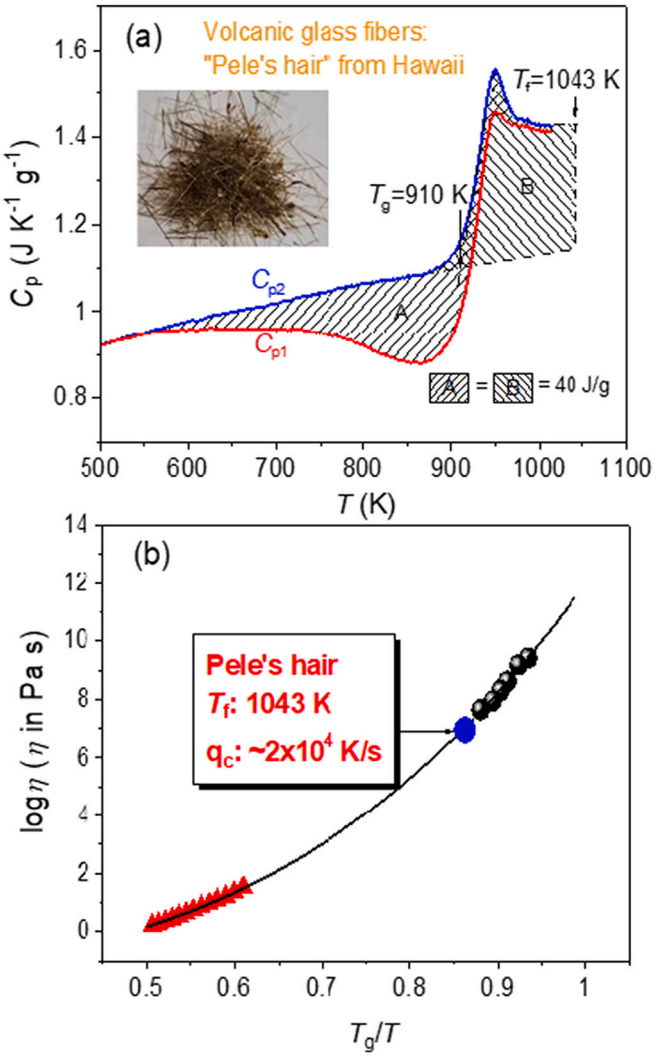

Fig. 2. Thermal history of "Pele's hair" (volcanic glass fibers) determined using the three-steps approach (unpublished data). **(a)** Determination of the fictive temperature (T_f) of Pele's hair using the "energy bird" through the enthalpy matching method. Inset: Image of the Pele's hair found in Hawai'i Island. **(b)** Determination of the cooling rate of Pele's hair through the relation between the logarithmic viscosity (η) and the T_g scaled temperature, T_g/T.

At the Annual Meeting of the International Commission on Glass in Brazil in 2003, for the first time I presented the determination of the thermal history of Pele's hair. Five years later, Potuzak et al. [32] also measured the characteristics of Pele's hair, including fictive temperature and cooling rate, using the three-steps approach [8]. The present article is a good place to show these unpublished data on Pele's hair (Figs. 2a and b), thereby confirming that the three-steps approach is an effective way to reveal the thermal history of HQ glasses. In 2017, Zhang et al. applied the three-steps approach to identify the effect of the fiberizing method on the mechanical properties of the filtration mats consisting of glass wool fibers [50]. In 2018, Deubener's group determined the thermal history of the wet-granulated blast furnace slag (a kind of HQ glass) by using the three-steps approach [57]. In 2019, Wuttig's group reported that the three-steps approach was successfully utilized to estimate the real T_g value of a chalcogenide glass with high tendency to crystallize [58]. Otherwise, it would be impossible to determine the real T_g of this glass since it crystallizes below T_g, that is, crystallization obscures the glass transition. In their paper in the present Angell issue, Lucas et al. have inferred the real T_g value of glassy water by subjecting the 'energy bird' to annealing and by performing the Kissinger analysis of the crystallization kinetics [59].

3.3. 'Energy bird' as signature of structural heterogeneity

Figs. 3a-c demonstrate the sensitivity of the 'energy bird' for HQ calcium silicate wool fibers to variation in chemical composition, specifically, to x in (100-x)SiO_2·xCaO (mol%), i.e., to the CaO fraction. For $x = 34$ and 40, the 'energy bird' is severely distorted (see Figs. 3a and b), particularly the head of the 'energy bird' greatly differs from that of the 'normal bird' (Figs. 1a and 2a). Specifically, the C_{p1} curves deviate from the C_{p2} curves (i.e., C_p curves of the standard samples cooled at 0.333 K s^{-1}). It is clearly seen in Figs. 3a and b that three exothermic sub-events (i.e., peaks 1, 2 and 3) occur in the samples with x = 34 and 40, whereas only peak 1 can be observed for the sample with x = 55. This means that, besides the overall structural relaxation (reflected by the entire 'energy bird'), three sub-relaxation processes take place at different temperatures (Figs. 3a and b) since the energy barriers for the three structural relaxation events are different. Based on these phenomena, we infer that three structure domains (or clusters) represented by their respective relaxation peaks are present in the sample and exhibit different structural stabilities and different potential energies. In detail, the stability of the structure domains can be ranked in the sequence: peak 3 > peak 2 > peak 1 since the relaxation temperature follows the same sequence. The size of those clusters can be ranked as peak 3 > peak 2 > peak 1, by comparing the amount of the released energy (i.e., peak areas) among the three peaks. Furthermore, the 'energy bird' for the $x = 55$ sample is much less distorted and is nearly like a normal 'energy bird' (Fig. 3c), and exhibits only peak 1, which is significantly weaker than those for the x = 34 and 40 samples. This indicates that the energetic and structural heterogeneities decrease with increasing CaO content.

Since these peaks represent exothermic events, the relaxation of the structure domains (or clusters) must be ascribed to the disorder-order transition, implying that the three types of clusters are structurally disordered. The co-existence of different structure domains reflects the structural heterogeneity in HQ calcium binary glasses. However, the detailed chemical and structural features (e.g., the coordination

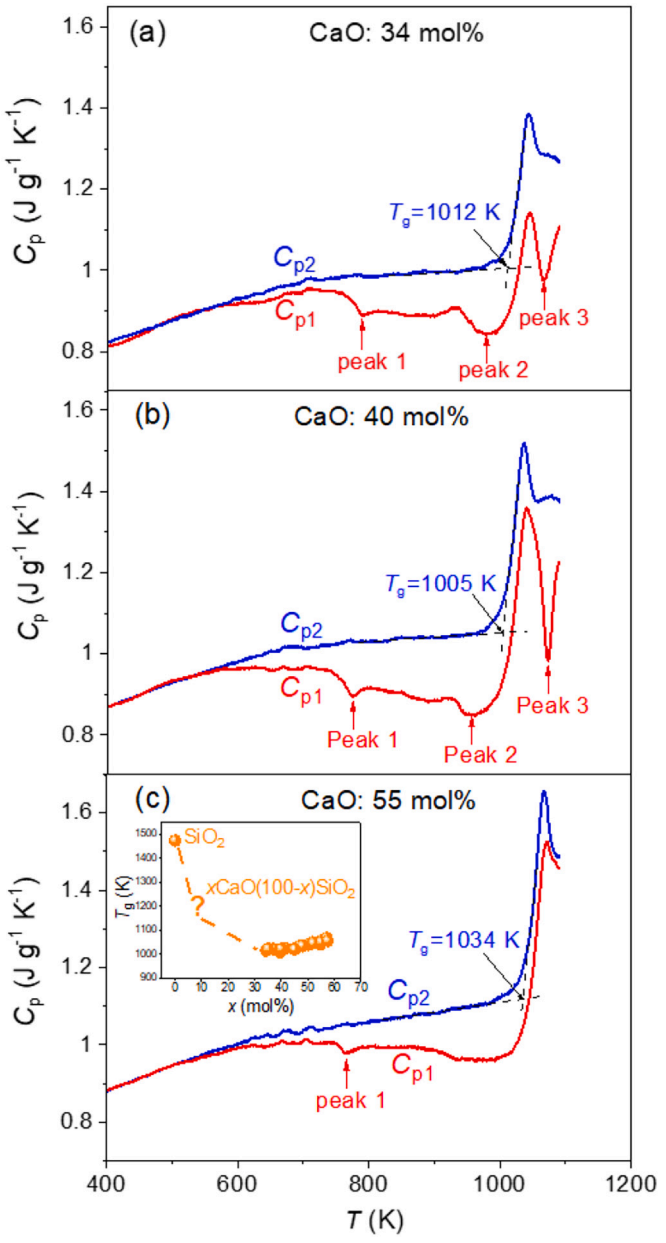

Fig. 3. The isobaric heat capacity curves, C_{p1} and C_{p2}, of the glass wool fibers with the compositions of xCaO-(100-x)SiO_2 (mol%), where x = 34 mol **(a)**, 40 mol% **(b)**, 55 mol% **(c)**, which were measured during the first and second DSC upscans at 0.333 K s^{-1}, respectively. The fibers were cooled at about 10^6 K s^{-1}. Reproduced with permission from [29]. Inset in Fig. (c): Impact of CaO fraction on T_g (unpublished data).

environment around Ca and Si) are not clear at this stage and need to be further clarified by other means such as microscopic and vibrational spectroscopic techniques.

As shown in Figs. 3a-c, during the second (standard) DSC upscan, both the excited network structure and the three kinds of clusters relax towards the average potential energy level of the standard glass. Consequently, the hyperquenching history of the three wool samples has been erased by the second upscan, and the structural heterogeneity is lowered. But those clusters are still embedded in the primary glass phase after the second upscan. These results suggest that the clusters in the fresh samples have the excessive potential energy relative to the average energy level of the primary glass phase.

It should be mentioned that those clusters could be eliminated if the melting temperature is sufficiently high. Interestingly, the amount of the clusters in the binary calcium silicate liquid can be decreased by increasing the CaO/SiO_2 ratio, i.e., an increase of CaO benefits the liquid homogenization. It is known that the structural heterogeneity depends on the topological arrangement and the distribution of silicon, calcium, and oxygen in the liquid at $T = T_f$. The co-existence of different types of clusters is a manifestation of nano-phase separation or nanoclustering in these studied liquids. Such phenomenon occurs also in many other glass-forming systems [60–62]. But it is still not known whether the phase separation observed in $CaO\text{-}SiO_2$ system is a density-driven process (polyamorphic transition) or a composition-driven process. In addition, it is not clear whether the tiny bump on the left side of peak 2 (Figs. 3a and b) is an endotherm or not, and what causes it.

The inset of Fig. 3c shows an interesting non-monotonic trend of T_g with varying CaO fraction, i.e., first drastically drops from the 1473 K of T_g for vitreous silica to 1012 K for the x = 34 sample, then increases to 1067 K for the x = 57 sample. However, the data in low and high x regions are still missing owing to the difficulty both in glass formation and in viscosity measurements. The T_g trend with composition indicates that the T_g depends not only on the network connectivity and bond strength, but also on the CaO clustering [61]. Thus, we can infer the origin of the T_g trend as follows. The drastic drop of T_g with increasing CaO in the low CaO content region arises from the increase of the number of non-bridging oxygen per SiO_4 tetrahedron, leading to dissociation of the structural network. In contrast, the slight increase of T_g with increasing CaO in the high CaO content region might be attributed to clustering of CaO, and the latter causes a reconnection of some of the tetrahedral [SiO_4] units within the intermediate-range order. To verify this conjecture, we need to acquire the accurate T_g trend in an extended range of CaO fraction. To do so, we need to design a special glass fabrication process for the calcium silicate compositions with poor glass forming ability.

When adding Al_2O_3 to the $CaO\text{-}SiO_2$ system, the calcium aluminosilicate (CAS) glasses can be obtained by rapid melt-quenching. We demonstrated that there is a high degree of structural heterogeneity at intermediate-range order (IRO) in CAS glasses [63]. We schematically proposed the scenario of structural arrangements in these glasses as shown in Figs. 4a and b. Fig. 4a illustrate the structural configuration based on the random IRO model. It was found that it was impossible to reproduce the ^{29}Si MAS NMR spectra by using the R-IRO model (Fig. 4a). In contrast, our quasi-heterogeneous IRO model (Fig. 4b) was able to convincingly match the NMR spectra, implying the co-existence of two types of structural domains (clusters) in the network structure. One type is the depolymerized SiO_4 domains with a certain number of non-bridging oxygens (see the red area), the other is the polymerized clusters of alternating SiO_4 and $(0.5Ca)AlO_4$ units (see the black squares). It was found that the fraction of the intermediate-range clusters increases as the contents of both Al and NBO increase, suggesting that the degree of heterogeneity increases. The observed IRO heterogeneity may explain the compositional dependence of both viscous behavior of CAS liquids and the stability of CAS glasses against crystallization. It should be mentioned that the IRO domains are present in the liquid state and can be trapped in the glass state by fast quenching [64].

Fig. 5 shows a scenario where the quenching rate affects the crystallization behavior of a fluoroapatite glass. It is evident that the fast cooled glass (i.e., the glass obtained by pressing the corresponding melt using a copper block) exhibits an ‘energy bird’, while the slowly cooled glass (i.e., the glass achieved by casting its melt onto a graphite mold) displays only a minor energy release peak. It is also seen that the crystallization events start already before the end of the glass transition, indicating that the studied apatite composition is a poor glass former. According to our previous study [33], some tiny crystals with size of 200–500 nm already exist in the original glasses. However, the fast cooled glass exhibits a stronger crystallization tendency during reheating, compared with the slowly cooled glass, as the crystallization peak of the former is considerably stronger than that of the latter. This gives the following three implications. First, the fast cooled glass contains more

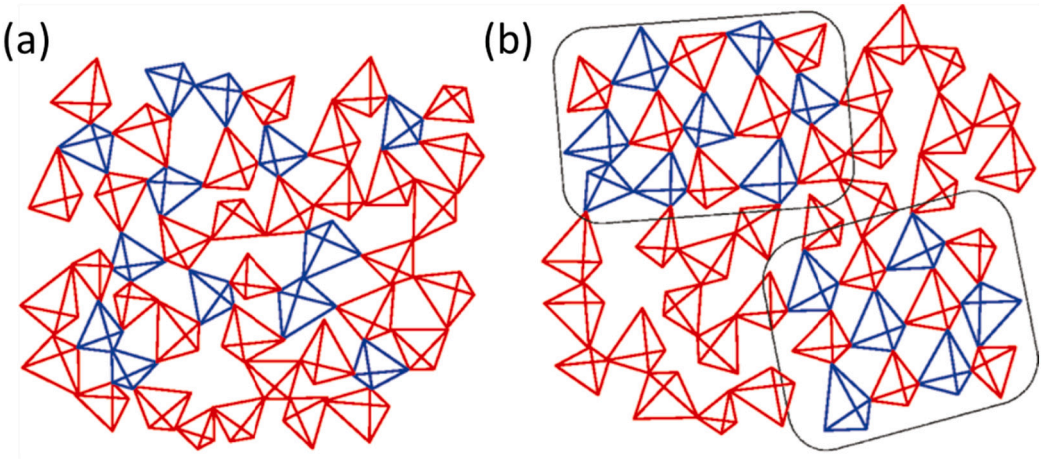

Fig. 4. Schematic plot of the intermediate-range structure of the CaO-Al_2O_3-SiO_2 glasses in two dimensions. Red: SiO_4 tetrahedral units; Blue: $(0.5Ca)AlO_4$ tetrahedral units. Oxygen ions lies in the four corners of the tetrahedra. **(a)** Structural arrangement based on the random intermediate range order model; **(b)** Structural arrangement according to the quasi-heterogeneous IRO model. Squares: The polymerized regions of alternating SiO_4 and $(0.5Ca)AlO4$ units. (For interpretation of the references to colour in this figure legend, the reader is referred to the web version of this article.)

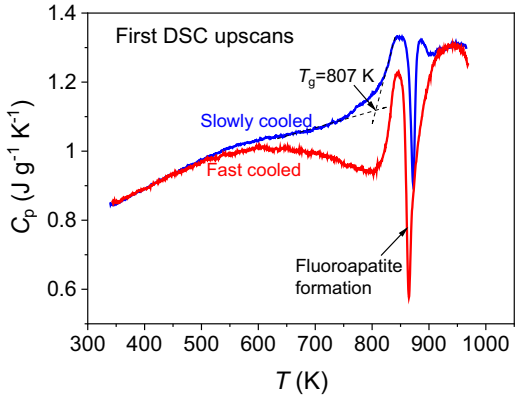

Fig. 5. Influence of the sub-T_g enthalpy relaxation on the subsequent crystallization peak, which is related to the fluoroapatite formation in the glass. The C_p curves were obtained for the first DSC upscans at 0.333 K s^{-1} for both the slowly cooled (blue curve) and the fast quenched (red curve) samples. (For interpretation of the references to colour in this figure legend, the reader is referred to the web version of this article.)

glass phase than the slowly cooled one prior to reheating, and hence the former undergoes a greater extent of crystallization than the latter. Second, the thermal history (cooling rate and T_f) of glass can greatly influence the crystallization behavior. Third, the studied apatite glass involves a high degree of structural heterogeneity that lowers the energy barrier for nucleation to occur. The above results are consistent with the trend observed in our previous studies [46,47]. That is, the structural heterogeneity in glass has a strong impact on the sub-T_g relaxation behavior and the glass forming ability.

Recently we detected the structural heterogeneity in the metal organic framework glass - ZIF-62 glass by using the annealing-DSC scanning approach [65]. Specifically, as shown in Fig. 6, we observed how and to what extent the glass transition overshoot of ZIF-62 glass evolves with annealing duration (t_a) at a given temperature (T_a) between 553 and 587 K, i.e., between 0.93 and 0.99T_g or with varying T_a at a given t_a. Fig. 6a shows the C_p curves of ZIF-62 glass annealed at $T_a = 559$ K for various durations (t_a). It is seen that the glass transition overshoot gradually increases with extending t_a, but the T_g value (i.e., the onset temperature of the glass transition) remains unchanged (around 593 K). This implies that the overshoot enhancement is not attributed to the primary (α) relaxation, instead, is associated with the secondary (β) relaxation [65,66] (see the next section). In terms of PEL, floppy structural units (e.g., organic ligands) gradually enter local minima with lower configurational entropies during sub-T_g annealing, compared to

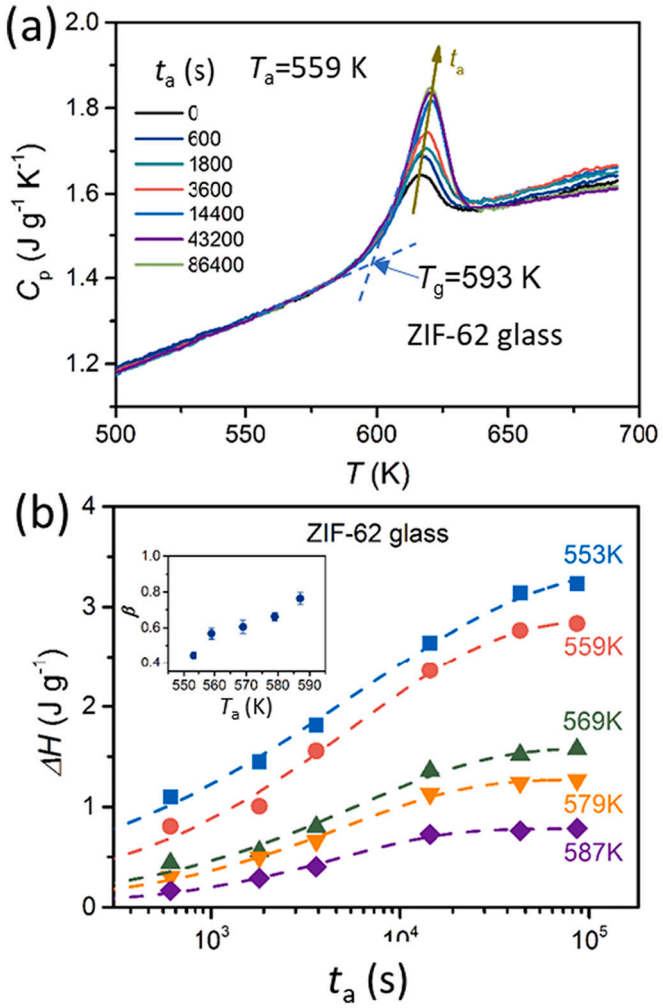

Fig. 6. Impact of the sub-T_g annealing on the overshoot of the glass transition (GT) and the stretch-exponent (β) of the Kohlrausch function of the enthalpy relaxation for the metal-organic framework glass: ZIF-62 glass. **(a)** The C_p curves of ZIF-62 glass annealed at $T_a = 559$ K for different durations (t_a), which were measured at 0.167 K s^{-1}. **(b)** The enthalpy (ΔH) of the GT overshoot as a function of t_a at various temperatures below T_g. Inset: T_a dependence of the stretching exponent β. Reproduced with permission from [65].

the rigid units (e.g., ZnN_4 tetrahedra). The energy barriers between such local minima need to be overcome for the floppy units to return to the average potential energy level of the standard glass (i.e., glass cooled at 0.167 K s^{-1}) during DSC upscanning. This process requires kinetic energy to be transferred from the environment to the glass sample, leading to the glass transition overshoot. In addition, the area of the overshoot, i.e., the recovered enthalpy, of glass transition peak increases with extending t_a. This means that, upon annealing, some structural units in glass fall to the potential energy level below that of the standard glass. The energy released from ZIF-62 glass during annealing is regained by reheating the glass in DSC at the standard rate of 0.167 K s^{-1} and consequently the sample becomes a standard glass.

The enthalpy (ΔH) recovered during annealing was determined by integrating the C_p difference between the glass samples with $t_a > 0$ and the not-annealing one over the temperature range from the onset to the offset of the glass transition. Fig. 6b exhibits the t_a dependence of ΔH at different T_a. It is observed that ΔH increases with t_a at a given annealing temperature below T_g and decreases with T_a for a given annealing duration. The time dependence of the recovery enthalpy for ZIF-62 glass can be fitted by the Kohlrausch–Williams–Watts (KWW) function [66]. By fitting, we can obtain the stretching exponent β, which is a measure of the distribution width of the relaxation time, ranging from 0 to 1. The inset of Fig. 6b shows that the β value of ZIF-62 glass increases from 0.44 to 0.76 when T_a is raised from 0.93 to 0.99T_g. This is a considerably broader range of β values for the T_a range compared to other glass formers shown in [65]. The stronger T_a dependence of β value implies that a high degree of structural heterogeneity exists in ZIF-62 glass, which could be related to a high degree of short-range disorder in this glass [67].

Controlling the structural heterogeneity of glass is crucial in designing the functional glasses and for tuning the properties of glasses, since the structural heterogeneity is a precursor for both phase separation and nucleation in glass. A recent study demonstrated that the structural heterogeneity promotes nano-phase separation in an oxide glass system containing the components of the perovskite crystals, by means of ultrafast laser radiation [60]. Such nano-phase separation led to the subsequent precipitation of perovskite nanocrystals in the glass matrix, and the composition and bandgap of these crystals could be tuned by varying the laser radiation condition. Consequently, the 3-dimensional lithography of PNCs in glass was realized. Another study [68] showed that the structural heterogeneity was advantageous to the precipitation of nanocrystals in the vanadium tellurite glass anodes for lithium-ion batteries (LIBs) upon charging/discharging cycling. These nanocrystals cause a significant enhancement of the cycling stability of LIBs. Recently we reported that the structural heterogeneity in MOF glass anodes enhanced the electrochemical performances of LIBs [69]. This is because the heterogeneous structure could readily be dissociated during charging/discharging cycling, thereby increasing both the active sites and the channels for lithium-ion storage and transfer.

Glass transition is characterized by an abrupt drop of the configurational entropy in a supercooled liquids during cooling, which is accompanied by an increase of structural heterogeneity. Recently, Tong and Tanaka found the connection between the temperature/density driven dynamics and the structural order parameter for supercooled liquids [70]. Jug et al. gave a detailed discussion on the spatial heterogeneities of supercooled liquids and glasses and their connection to physical properties [71]. According to their study, glasses can be described as dynamically arrested heterogeneous supercooled liquids with both solid-like and liquid-like nanoscale regions. The heterogeneities exhibit different size distributions with the solid-like regions that involves hidden quasi-order. The link between these size distributions and the features of the 'energy bird' will be an important subject to be investigated in future. Seeking such a link can help us to enhance physical properties and functionalities of glasses.

3.4. Shadow glass transition

As mentioned above, a HQ glass is a system far from equilibrium with a fictive temperature significantly higher than its T_g. When a HQ glass is annealed below T_g for a certain period and then undergoes two DSC upscans, a series of energy release events can be observed as shown in Figs. 7a-c. The evolution of the 'energy bird' with annealing temperature

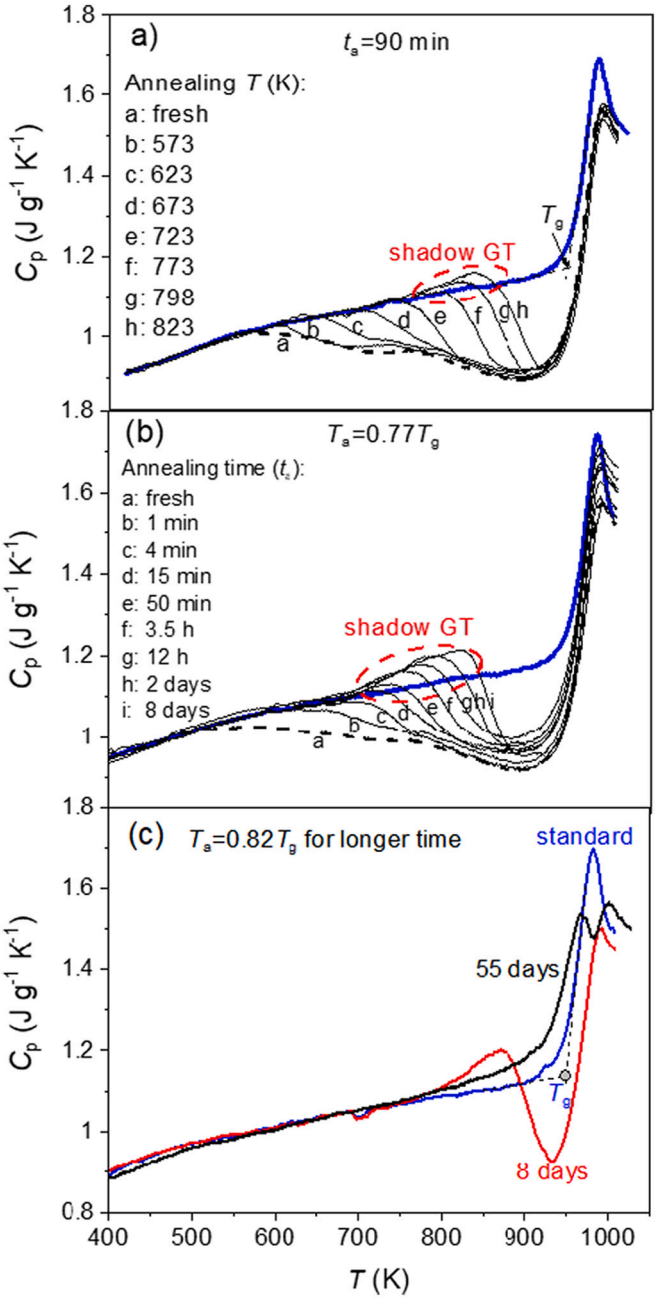

Fig. 7. The impact of sub-T_g annealing on the 'energy bird' of stone wool sample (discontinuous glass fibers hyperquenched at $>10^6$ K s^{-1}). **(a)** Annealing temperature (T_a) effect for t_a = 90 min. Reproduced with permission from Ref. 20. **(b)** Annealing time effect at the temperature of 0.77T_g (T_g = 950 K). Reproduced with permission from Ref. 36. **(c)** Annealing effect at 0.82T_g for longer time (t_a = 8 and 55 days) (new figure). Thick blue curves: the standard samples (cooled at the standard rate of 0.167 K s^{-1}); Dashed black curves: fresh HQ sample. All C_p curves were acquired during DSC upscans at 0.333 K s^{-1}. Red dashed ellipse: Shadow glass transition (Shadow GT) region. (For interpretation of the references to colour in this figure legend, the reader is referred to the web version of this article.)

(T_a) and time (t_a) dispalys several features that are critical in understanding the sub-T_g relaxation and the glass transition, as well as in optimizing physical properties of glass products. The shape of the annealed 'energy bird' depends on the chemical composition and liquid fragility of glass systems [30,45]. Most of the previous studies about enthalpy relaxation focused on 'normally' cooled glasses, i.e., bulk glasses. In recent years, several research groups have been investigating the relaxation behavior of HQ glasses such as thin glass fibers and metallic glass ribbons. Such investigations provide abundant information on dynamics and thermodynamics of glass transition. In 2004, Yue and Angell came up with the term - shadow glass transition, when they studied the sub-T_g enthalpy relaxation in hyperquenched (HQ) glasses [20,24]. Here I review recent progress in exploring the dynamic and structural origin of the shadow glass transition based on Figs. 7 to 9.

Fig. 7a shows the impact of the annealing temperature (T_a) on the 'energy bird' for the typical HQ glass - stone wool fibers for the annealing time (t_a) of 90 min. It is seen that the left cutoff of the enthalpy release peak (i.e., the tail of the 'energy bird') gradually shifts to higher temperatures with increasing T_a. This implies that upon annealing the configurational states with higher potential energy are transformed into those of lower potential energy. When T_a is sufficiently high (but still below T_g), an endothermic pre-peak occurs right before the start of energy release. To some extent, this endothermic pre-peak displays similar features as the subsequent glass transition peak, and hence this pre-peak was named the shadow glass transition (shadow GT) [20,24]. The shadow GT peak of stone wool was compared with the detected endothermic peak of glassy water [6] to clarify the glass transition behavior of water [20,24]. Recently, Pries et al. [58] and Lucas et al. [59] inferred that the endotherms of both some chalcogenide glasses and glassy water, which appear prior to their crystallization peaks, should be the shadow GT events. Based on this inference, they derived their real T_g values by comparing the locations of the 'energy birds' of various HQ glass systems on the T/T_g axis. Although the assignment of the T_g value of water is under debate [3,5,6,20,24,59,72–78], shadow GT is an appealing feature of some extremely glass formers, which is critically important for understanding the potential energy landscape of glass-forming liquids, glass relaxation and glass transition. The onset temperature of shadow GT is here called the shadow T_g. The shadow GT peak becomes stronger with increasing T_a (Fig. 7a), but its onset remains the same. In contrast, the energy release peak becomes smaller with T_a. Both the shadow GT peak and the energy release peak can coexist for a certain range of T_a.

Fig. 7b shows that annealing time t_a has a similar effect on the 'energy bird' of stone wool at T_a = 723 K. If t_a is sufficiently long, the shadow GT peak appears, followed by an exotherm. The shadow GT peak becomes more pronounced with t_a and shifts to higher temperature until the exotherm disappears. This feature implies that, upon sufficient annealing, the potential energy of weakly bonded structural units in HQ glass drops to a level below that of the standard glass, and finally to that determined by the given T_a, whereas that of strongly bonded structural species remains higher than that of the standard glass. Fig. 7c shows the effect of the long annealing time (8 and 55 days) at 0.82T_g on the 'energy bird'. After 8 days annealing, the shadow GT peak is drastically enhanced, whereas, after 55 days annealing, the height of the shadow GT peak becomes nearly the same as that of the glass transition peak, as if twin glass transitions occur. But the reality is that the shadow GT is fundamentally different from the real GT in terms of their dynamical and structural origins. The shadow GT is irreversible during reheating [48], whereas the real one is reversible. Here the key question is: what causes the shadow GT peak?

To answer the above question, I have drawn Fig. 8 to illustrate what happens to the HQ stone wool, the composition of which is given in the experiment section, during hyperquenching, sub-T_g annealing and DSC upscanning. Afterwards, I describe a recent important finding of Haibin Yu's group, which deals with the origin of the shadow GT in metallic glass systems [79].

The left panel in Fig. 8 shows the $C_{p,exc}$ (=C_{p2}-C_{p1}) curve of the HQ sample annealed at 773 K (0.82T_g) for 1 day. It is seen that this annealing condition causes a huge endotherm, i.e., shadow GT, followed by an exotherm that reflects the energy release. As shown in the right panel of Fig. 8, the stone wool liquid is hyperquenched to glass state, accompanied by a drop in potential energy (see red down-arrow). However, the average potential energy of HQ glass is significantly higher than that of the standard glass (i.e., the glass cooled at 0.333 K s^{-1}). Upon 1 day annealing at 0.82T_g, a primary portion of the structural species in HQ glass relaxes, leading to the partially annealed glass state (see the light blue down-arrow). This process releases the potential energy, which is the difference between the total released energy, i.e., the area of the original 'energy bird' shown in Fig. 1b (see the black down-arrow) and the energy corresponding to the area of the exothermic peak (see the left panel of Fig. 8). At the same time, a minor portion of the structure species in HQ glass relaxes to the deeply annealed state via losing additional potential energy that equals to the area of the shadow GT peak (see the green down-arrow). During DSC upscanning, the lost energy is recovered to the level of the standard glass (see the blue up-arrow), and the remaining energy is released towards the level of the standard glass (see the blue down-arrow). The evolution of the potential energy shown in Fig. 8 is a clear signature of structural heterogeneity of glass.

Here it should be mentioned that, in addition to our observation of the shadow GT in oxide glasses, other researchers independently observed the endothermic pre-peak in other families of glasses including

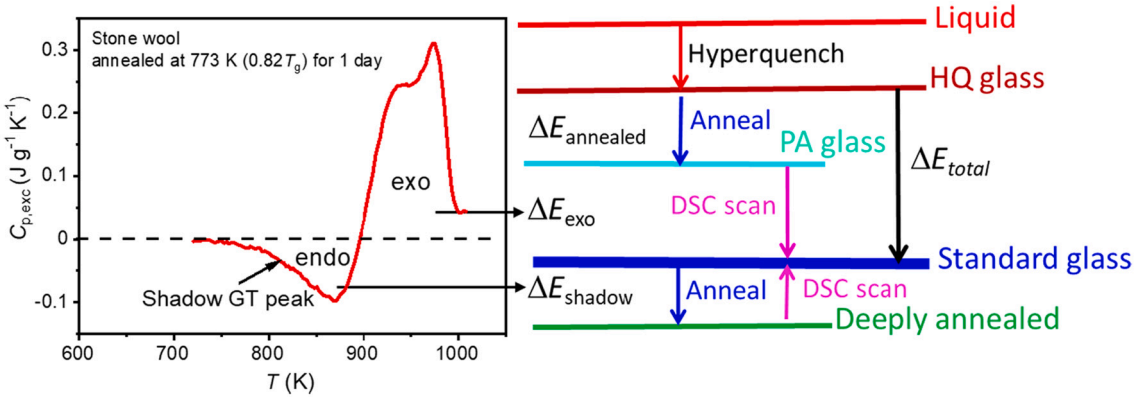

Fig. 8. Enthalpy evolution during sub-T_g annealing and DSC upscan. Left panel: The excessive heat capacity ($C_{p.exc}$) curve with a distinct contrast between shadow glass transition (shadow GT) and the enthalpy release peak for the stone wool annealed at 773 K (0.82T_g) for 1 day. The DSC upscans was conducted at 0.333 K s^{-1} in argon. Right panel: Schematic representation of the enthalpy change during hyperquenching, annealing and DSC upscan; PA glass: Partially annealed glass.

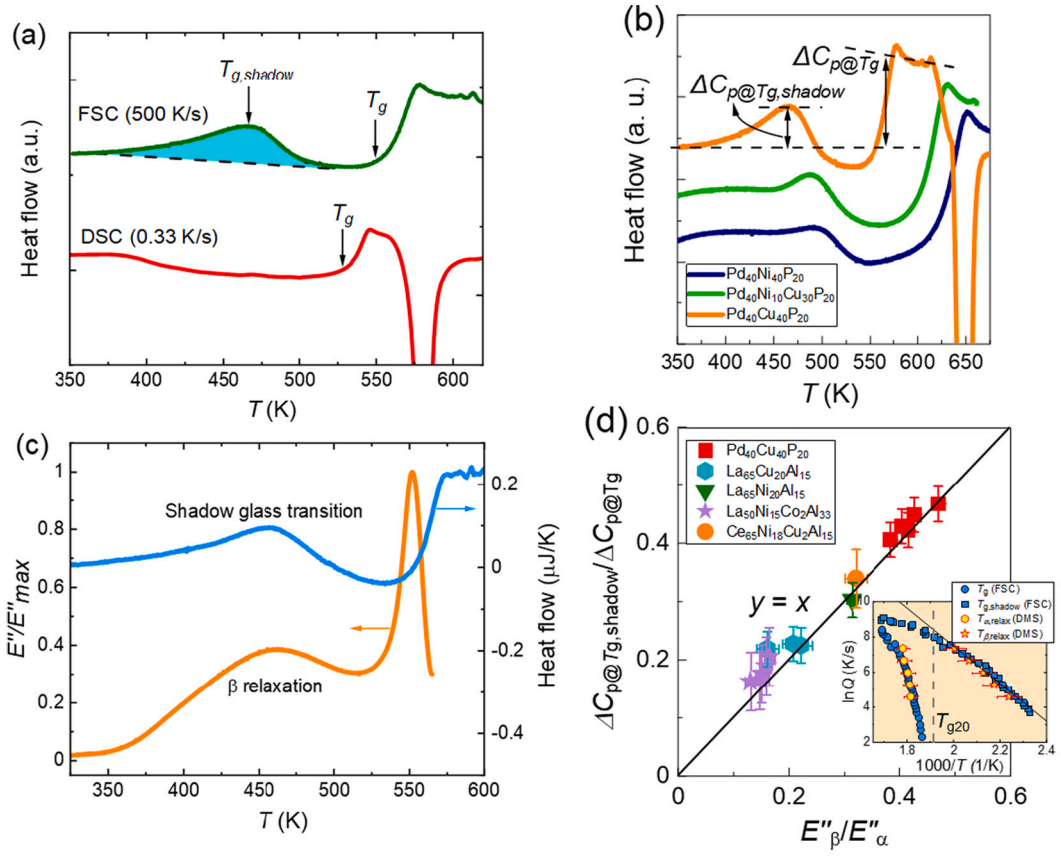

Fig. 9. The correlation between the shadow glass transition (Shadow GT) and β relaxation for several HQ metallic glasses. **(a)** Comparison between the heat flow curve obtained by conventional DSC at the upscan rate 0.333 K s^{-1} and that obtained by FSC at the upscan rate 500 K s^{-1} for HQ $La_{50}Ni1_5Co_2Al_{33}$ glass. **(b)** The FSC curves for the $Pd_{40}Ni_{40-x}Cu_xP_{20}$ (x = 0, 30 and 40) glass at 500 K s^{-1}, showing the extents of both shadow GT ($\Delta C_{p@Tg,shadow}$) and real glass transition ($\Delta C_{p@Tg}$). **(c)** FSC curve (at 200 K s^{-1}) versus DMS loss modulus curve (at 2 Hz). **(d)** Linear relationship between the scaled extent of shadow GT ($\Delta C_{p@Tg,shadow}/\Delta C_{p@Tg}$) and that of β relaxation (E''_β/E''_α). **Inset**: Relaxation map showing the β relaxation, α relaxation, shadow glass transition and real glass transition. The vertical dashed line ($T_{g,20}$) refers to the standard T_g measured at 20 K/min. Black solid line: the Arrhenius equation fitting to the β relaxation. Reproduced with permission from Ref. 79.

metallic glasses [80], organic glasses [81], and chalcogenide glasses [58,59]. According to Yue and Angell [20], the shadow glass transition arises from the energetic and structural heterogeneities in HQ glasses, which features a non-exponential relaxation trend. It is related to a non-monotonic decay of fluctuations in density and enthalpy in glass during annealing [82]. Due to its non-exponential nature, the shadow GT can also be described by the KWW function [66] and even more accurately by a generalized stretching function that we proposed in [83]. Intuitively, any glass can be regarded as being composed of many micro-domains, each of which possesses its own T_g. The shadow GT is a rejuvenation process (i.e., energy gain) of some domains in glass structure. In the sense of PEL, those energetically unstable domains or species (e.g., network modifiers in oxide glass) access deeper basins in PEL during annealing than the stable ones, consequently the potential energy of the unstable ones drops below the average potential energy level of the standard glass. Upon reheating, the unstable structural species in deeper basin of PEL absorb the kinetic energy provided by DSC to reach the energy level of the standard glass, thereby causing the shadow GT peak.

It has been established that the glass transition is associated with the primary relaxation, namely, α relaxation, which involves the cooperative rearrangement of large structural entities (e.g., network forming units), accompanied by a change of the configurational entropy (S_c). The size of the cooperative rearranging regions increases and S_c decreases when a liquid is transformed into glass state, and vice versa. In addition to α-relaxation, the secondary relaxation, i.e., β relaxation also occurs in glass during heating or cooling or isothermal annealing within a certain temperature window. β relaxation is associated with the local rearrangement of sub-structural network units towards lower potential energy states. These units are composed of modifiers bonded to oxygens in oxide glasses [84,85]. As reported previously, β relaxation was identified in HQ glasses by analyzing their 'energy birds' [53–55].

To reveal the origin of shadow GT, Yu's group recently performed a beautiful study, i.e., they utilized both the chip-based fast scanning calorimetry (FSC) and dynamic mechanical analyser (DMS) to detect both the thermal and the mechanical responses, respectively, of several HQ metallic glasses to dynamic heating [79,86]. They compared the enthalpy relaxation modes of HQ glasses with their mechanical relaxation modes to identify whether they relate to one another. Interestingly, as illustrated in Fig. 9a, they observed an endothermic pre-peak in the HQ $La_{50}Ni1_5Co_2Al_{33}$ glass, followed by an exothermic peak and then by a real glass transition peak, during the FSC upscan. Obviously, this endotherm is the shadow GT peak, meaning that the fast FSC upscan can generate shadow GT without prior annealing since FSC can provided a heating rate that is significantly higher (at least 3 orders of magnitude) than the conventional DSC (Fig. 9a). In contrast, the conventional DSC upscan can result in shadow GT only when a HQ glass is sufficiently annealed below T_g. This comparison indicates that the shadow GT is a much faster relaxation process than the primary relaxation process in the temperature range of the real glass transition.

By subjecting more HQ metallic glasses to FSC scanning, Yu's group verified that shadow GT is a universal feature of HQ metallic glasses (Fig. 9b) [79]. For the $Pd_{40}Ni_{40-x}Cu_xP_{20}$ glass series with $x = 0$, 30, 40, a crystallization peak appears after the end of the real glass transition. To figure out what kind of relaxation modes causes the shadow GT, they

compared the shadow GT peak of the FSC curve (measured at 200 K s^{-1}) with the β relaxation peak of the DMS loss modulus curve (measured at 2 Hz) in Fig. 9c and found that both peaks occur in the same temperature range (400–500 K). This implies that shadow GT is correlated with β relaxation.

As illustrated in Fig. 9b, the magnitudes of both the shadow GT and the real glass transition are quantified by the heights of the two peaks, i.e., $\Delta C_{p@Tg,shadow}$ and $\Delta C_{p@Tg}$, respectively. Fig. 9d shows the 1:1 proportionality between the extent of shadow GT and that of β relaxation. This is the first direct evidence for β relaxation being the dynamical origin of the shadow GT. Furthermore, the heating rate dependence of the shadow GT overlaps with that of β relaxation, while the heating rate dependence of the real glass transition merged with that of α relaxation above T_g (see the inset of Fig. 9d). These findings led to establishing the bridge between the dynamics and the thermodynamics of β relaxation. Interestingly, Yang et al. also discovered that the shadow GT temperature ($T_{g,shadow}$) first drops with increasing the quench rate, and then reaches a plateau when the rate exceeds 10^6 K s^{-1} [79]. This suggests that a critical $T_{g,shadow}$ value exists, below which the glass structural domains with the lowest potential energy cannot be rejuvenated to the average energy level of the standard glass.

Moreover, Yu's group discovered the direct correlation between β-relaxation and mechanical properties for the metallic glasses, specifically an enhancement of β-relaxation increases the microscale tensile plasticity [87]. They also found that the structural heterogeneity relates to β-relaxation in metallic glasses. This is an important step for revealing the structural and dynamic origin of the shadow GT. Certainly, the microscopic origin of the shadow GT still needs to be further explored. It is worth noting that, besides fast β relaxation, the Johari-Goldstein relaxation (i.e., slow β relaxation) [88,89] occurs in many glass formers such as GeO_2 glass [54] and metallic glasses [55]. These findings were achieved through the 'energy bird' approach.

To further clarify the shadow GT behavior, I should mention another important advance, which was recently achieved by Pries et al. on some chalcogenide glasses such as GeSe and $Ge_2Sb_2Te_5$ glasses [58]. These glasses are known as ideal phase-change materials for memory technologies. They observed the shadow GT in these glasses through two ways. One way was to anneal the glass below T_g at different temperatures for various durations, and subsequently to upscan the annealed sample in a conventional DSC. When these glasses are subjected to a certain degree of annealing (i.e., certain annealing temperature and duration) below T_g, the shadow GT occurred and became more evident with further annealing, being similar to the case shown in Fig. 7. To the best of my knowledge, this is the first observation of shadow GT for the family of chalcogenide glasses. The other way is to rapidly upscan the not-annealed glass by an ultrafast DSC, leading to appearance of a shadow GT peak. Through these elegant experiments, Pries et al. inferred that the T_g values of several phase-change materials reported in literature [90] were significantly underestimated, because the onset of the shadow GT was assigned as T_g. They found that $Ge_2Sb_2Te_5$ glass crystallized below T_g. To obtain the real T_g of $Ge_2Sb_2Te_5$ glass, they compared its 'energy bird' with those of other families of HQ glasses including organic, metallic, and molecular ones with respect to their location on the T/T_g axis. They identified that the $C_{p,exc}$ peaks of all the HQ glasses were located at T/T_g = 0.85–0.95. Based on this fact, they inferred that the T_g value of $Ge_2Sb_2Te_5$ glass should be about 473 K, which is 90 K above the previously assigned T_g (383 K).

In the present Angell issue, Lucas et al. discussed the glass transition of glassy water by considering the shadow GT in phase change materials [59]. By performing sub-T_g annealing and ultrafast DSC upscanning on $Ge_2Sb_2Te_5$ glass, they inferred that the onset (136 K) of the endotherm for HQ glassy water prior to crystallization [6] was not the real standard T_g, instead, the onset of the shadow GT. Through the Kissinger analysis of the crystallization kinetics, they confirmed that water crystallization occurred below T_g during dynamic heating [59]. Thus, their conclusions are in line with the findings reported in [5,20], in which the T_g of glassy water was estimated to be around 165 K, higher than the previously assigned value (136 K). Interestingly, Shephard and Salzmann found that the shadow GT of low-density amorphous water is associated with the 'molecular reorientation scenario' [78].

Here it should be pointed out that shadow GT does not occur in strong glass systems, i.e., the systems with low liquid fragility index ($m < 20$) [2], such as SiO_2 and GeO_2 (see Section 3.6). The lack of the shadow GT peak in strong glass formers implies that their energetic and structural heterogeneities are significantly lower than those in fragile glass formers. Since metallic glass-forming liquids are fragile systems, they exhibit shadow GT. In addition, Johari discussed the details about the features of the sub-T_g relaxation in glassy water [72,73].

3.5. Vibrational dynamics of HQ glasses

The atomic vibrational dynamics has a strong impact on physical properties of both glass and its correlated states: liquid, supercooled liquid and solid. In 2003, Austen initiated an exciting collaboration project, in which I participated, with respect to the impact of sub-T_g annealing on the vibrational density of states (VDOS) in a HQ glass (stone wool) [9]. It is known that an intriguing feature of VDOS in disordered materials is the excess of low-frequency states relative to those predicted by the Debye theory. These excessive VDOS manifests itself in the incoherent inelastic neutron scattering or the Raman spectra as the Boson peak, between 2 and 10 meV. Its intensity depends on temperature, pressure, density, and chemical composition. Although the Boson peak is related to the intermediate-range order, its structural origin is still under discussion [9,35,91]. It is known that distinct configurational excitations in glass involve structure change and defect formation, and hence, low-frequency modes, presumably with a transverse character [9]. These modes depend on the density change of glass [35,91]. It should be stressed that the density change induced by pressure is associated with local structural changes in glass [10].

Since stone wool possesses significantly higher potential energies than a standard sample, it is an ideal material to understand the Boson peak in terms of low-frequency modes involving nanoclusters, defects, mismatching or connected rings or small tetrahedral rocking groups. In addition, stone wool has a fictive temperature well above T_g, and thus the structure of its corresponding supercooled liquid can be probed without any adverse effects from quasi-elastic scattering [9,25]. For this purpose, the cold-neutron inelastic scattering with time-of-flight measurements was used because its output, $Z(\omega)$, can be approximately regarded as a measure of the vibrational density of states (VDOS) if those effects like multiphonon and multiple scattering can be ignored. Fig. 10

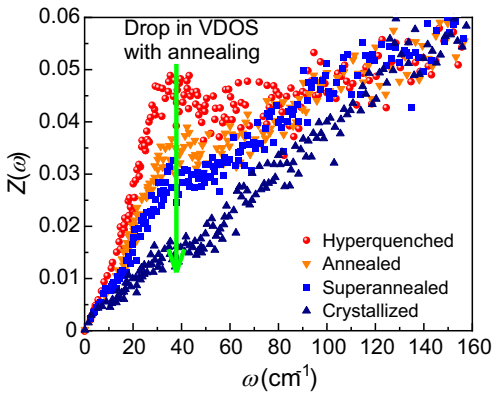

Fig. 10. Impact of the annealing degree on the vibrational density of states (VDOS) for stone wool. The VDOS was obtained by conductin cold-neutron inelastic scattering measurements. 'Hyperquenched': quenching at ~10^6 K s^{-1}; "Annealed": dynamically heating to above T_g and then cooling it at 0.167 K s^{-1}; 'Superannealed': annealing at 894 K (0.94T_g) for 21 h; 'Crystallized': isothermally treating at 1156 K for 2.5 h. Reproduced with permission from [9].

clearly shows that the intensity of the Boson peak at the ω value of about 40 cm^{-1} decreases from the level of the HQ sample to that of the super-annealed one with increasing the degree of sub-T_g annealing, i.e., with decreasing T_f [9]. Upon heat-treatment at 1.22T_g for 2.5 h, the stone wool sample crystallizes, and consequently the Boson peak vanishes. According to Angell et al. [9], the Boson peak can be regarded as a signature for the topologically diverse defects in glasses. These defects exist in the intermediate-range-ordered regions with the length scale of 9–16 Å. However, scientists still have different views about the source of the Boson peak for HQ glasses [9,35,91,92]. Here I describe two cases, in which I was involved, to illustrate the possible sources of the excessive VDOS shown in Fig. 11 and in Ref. 91.

In 2006, Monaco et al. studied the VDOS of both the HQ and the annealed $74SiO_2$-$16Na_2O$-4CaO-6FeO (SNCF) glass, where 30% of iron is enriched in the resonant ^{57}Fe isotope, by means of nuclear inelastic scattering [35]. Fig. 11a shows the 'energy bird' for the rapidly quenched SNCF glass. The size of the 'energy bird', i.e., the area between the two C_p curves (37 J g^{-1}), represents the excess of the potential energy in the glass relative to that of the standard sample. The T_f of the HQ SNCF glass was found to be 929 K (1.18T_g), whereas the T_f of the annealed SNCF glass is 770 K (see the inset of Fig. 11a), which is lower than T_g (786 K).

As shown in Fig. 11b, the reduced VDOS in the HQ sample at 5 meV is 19% higher than that of the annealed one. Here the question is: what is the origin of this difference? According to the Mössbauer spectroscopy and X-ray scattering, quenching or T_f has no detectable effect on the intermediate-range structure in SNCF glass. However, both the density and the sound velocity for the quenched SNCF glass are lower than those for the annealed one, meaning that T_f affects the macroscopic parameters. This suggests that the observed transformation of the reduced VDOS could be described by that of the elastic medium. The magnitude of the quenching effect on VDOS is close to that described in terms of the energy landscape [93] in glasses for a comparable T_f change. The similar quenching effect can be interpreted by the difference in the Debye energies.

Interestingly, when VDOS is renormalized after rescaling the energy axes in the Debye energy unit, the VDOSs for both samples become almost overlapped as shown in Fig. 11b. This confirms the role of the elastic medium. In other words, T_f does not affect the intensity of the Boson peak that is defined as the relative excess of states above the Debye level. The increase of the number of VDOS is compensated by a corresponding increase of the Debye level.

In 2014, an international team led by Chumakov conducted important experiments concerning the role of disorder in thermodynamics and atomic dynamics of glasses and the origin of the Boson peak of SiO_2 glass by using two techniques - nuclear resonant analysis of inelastic x-ray scattering and inelastic x-ray scattering [91]. Their results show that the VDOS in SiO_2 glass is excessive over that of the typical crystal like α-quartz. In addition, SiO_2 glass has an excess of heat capacity relative to that of the crystal. Remarkably, when they compressed the SiO_2 glass to make density equal to that of its counterpart SiO_2 crystal, the difference in both VDOS and heat capacity vanished. Based on these results, Chumakov et al. inferred that both the Boson peak and the higher heat capacity of SiO_2 glass compared to its counterpart crystals are not ascribed to disorder, but to a lower density [91]. Thus, the suppression of the Boson peak in stone wool upon annealing (Fig. 10) might also be caused by an increase of the sample density. However, to further confirm the inference in [91], it will be important to compress the HQ stone wool to match its density with that of the crystalline stone wool and to determine and compare their VDOS to see whether their VDOS become identical. It is worth noting that the change of the VDOS with varying T_f provides the information on the atomistic vibrational dynamics, but not on the structural heterogeneity.

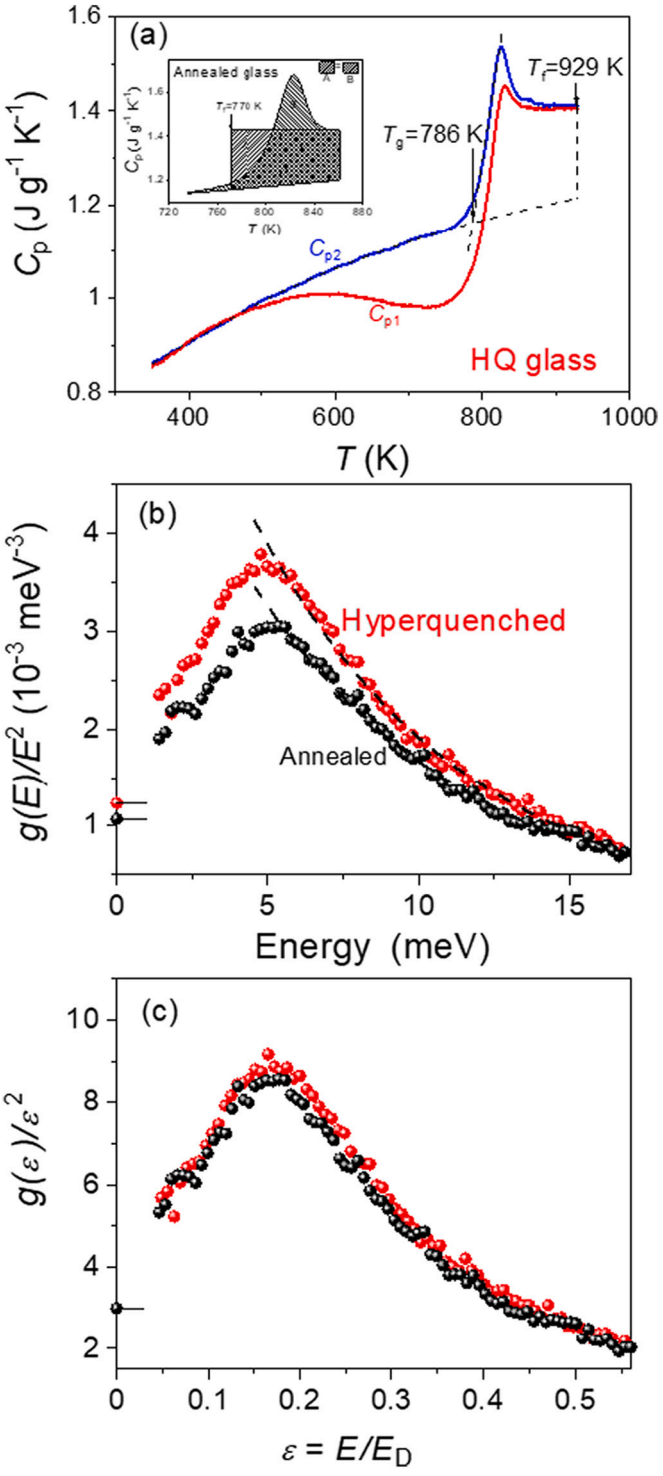

Fig. 11. Impacts of both hyperquenching and annealing on the reduced VDOS for the glass with the composition (wt%) of $74SiO_2$-$16Na_2O$-4CaO-6FeO. **(a)** 'Energy bird' obtained at a quenching rate of about 2×10^3 K s^{-1}. Inset: The C_p curve for the glass annealed at 785 K for 30 min and cooled at 3×10^{-2} K s^{-1}. T_f values for both the hyperquenched and the annealed samples, as well as T_g value of the standard sample are indicated. Inset: unpublished data. **(b)** Reduced VDOS in absolute units for both fast quenched and annealed glass. Dashed lines: The exponential decrease of the reduced DOS. The symbols and horizontal lines at $E = 0$: the calculated Debye level. **(c)** After rescaling the energy axes in Debye energy units and renormalization of the DOS area. Reproduced with permission from Ref. 35.

3.6. Impact of liquid fragility on the sub-T_g relaxation

It was Austen who proposed the generalized liquid fragility concept [94], according to which the glass-forming liquids can be classified into the "strong" and "fragile" categories. It should be mentioned that the liquid fragility here is the dynamic property of a glass forming liquid, i.e., the viscous slowing-down rate of a supercooled liquid at T_g upon cooling. The liquid fragility should be distinguished from the mechanical fragility of glass. Liquid fragility is usually quantified by the kinetic fragility index m, i.e., the slope of the $\log_{10}$(viscosity) ~ T_g/T curve at T_g [2]. In 2001, Austen's group discovered the direct correspondence between the liquid fragility and the thermodynamic fragility [4].

To investigate the influence of the liquid fragility on the sub-T_g relaxation, the relatively fragile system - stone wool (liquid fragility index $m = 51$), was compared with the typical strong system – SiO_2 ($m = 20$) concerning the relaxation patterns, i.e., the excessive heat capacity ($C_{p,exc}$) curves in Figs. 11a-f. To make a reasonable comparison, $C_{p,exc}$ is plotted against the T_g scaled temperature, T/T_g. Moreover, the T/T_g ratio also tells how far the temperature of the energy release peak is away from the standard T_g. Note that stone wool and SiO_2 fibers were obtained by hyperquenching at approximately 10^6 and $10^{5.5}$ K s^{-1}, respectively. By the comparison, we have identified 6 main differences in the sub-T_g enthalpy relaxation between the fragile and the strong glass forming systems as given below.

Difference 1: Shape and width of the energy release peak ($C_{p,exc}$ peak obtained from 'energy bird).

Stone wool exhibits a broader and less symmetrical $C_{p,exc}$ peak (Figs. 12a) than HQ SiO_2 (Figs. 12b), implying that the distribution of the kinetic energy that triggers the energy release of a fragile system is significantly broader compared with a strong system. Furthermore, the difference also indicates that a fragile system has more configurational microstates than a strong one. From a microstructure perspective, a fragile system involves more diversified chemical and structural species than a strong one. Each of these species has its own potential energy, which can be trapped in the glass state by hyperquenching its corresponding liquid state. Upon reheating at 0.167 or 0.333 K s^{-1}, those species will demand different kinetic energy (i.e., heating temperatures) to release the trapped energy. In stone wool composition, there are various types of network modifiers such as CaO, MgO, Na_2O, K_2O, and network forming oxides like SiO_2 and Al_2O_3, and hence, both the coordinated oxygen numbers of cations and the cation-oxygen bonds strength are diversified. In contrast, there exists only one type of network former (SiO_2) in SiO_2 glass, and hence, only one type of chemical bond (Si—O). However, there are still distributions of both the bond angles and bond lengths in SiO_2 glass although they are much narrower than in multi-component glasses like stone wool. This is why the sub-T_g relaxation in HQ SiO_2 occurs in a temperature range even though its $C_{p,exc}$ peak is narrower than that of stone wool for a given T_f/T_g ratio, i.e., for a comparable cooling rate (Figs. 12a and b). Note that the distribution of the potential energy in any glasses, and hence, the $C_{p,exc}$ peak becomes broader when T_f is increased. Compared with a lower T_f glass, a higher T_f glass exhibits not only a high average potential energy, but also a higher degree of structural 'distortion' and a larger number of the exited configurational states. If the heating time is shorter than the relaxation time, the distorted state of the glass structure will remain. Otherwise, the structure species would relax from the exited configurational states to those of the 'standard' glass that has a T_f value equal to T_g, resulting in an energy release.

Difference 2: Deconvolution of the energy release peak.

The $C_{p,exc}$ peak of stone wool is composed of a "shoulder" and a primary peak (Fig. 12a), whereas that of HQ SiO_2 is comprised of only one primary peak (Fig. 12b). The sub-T_g relaxation peak of stone wool can be well deconvoluted into two Gaussian peaks (i.e., peaks 1 in low T region and peak 2 in high T region, respectively). Peak 1 is associated with β relaxation, i.e., the fast relaxation of the network modifiers towards lower energy state [36,84], while peak 2 is correlated with α relaxation, i.e., the relaxation of the structural network composed of tetrahedral SiO_4 and AlO_4 units. In contrast, the $C_{p,exc}$ peak of HQ SiO_2 can be fitted by only one Gaussian function (Fig. 12b) [36], clearly indicating that only one distribution of relaxation time exists in strong systems, and the structural and energetic heterogeneities are less than those in fragile systems. The single Gaussian peak in Fig. 12b could be associated with the narrow distributions of the Si-O-Si and O-Si-O bond angles and lengths. The difference in the sub-T_g relaxation pattern between stone wool and HQ SiO_2 is consistent with that in PEL between fragile and strong systems. That is, a strong system features the PEL with

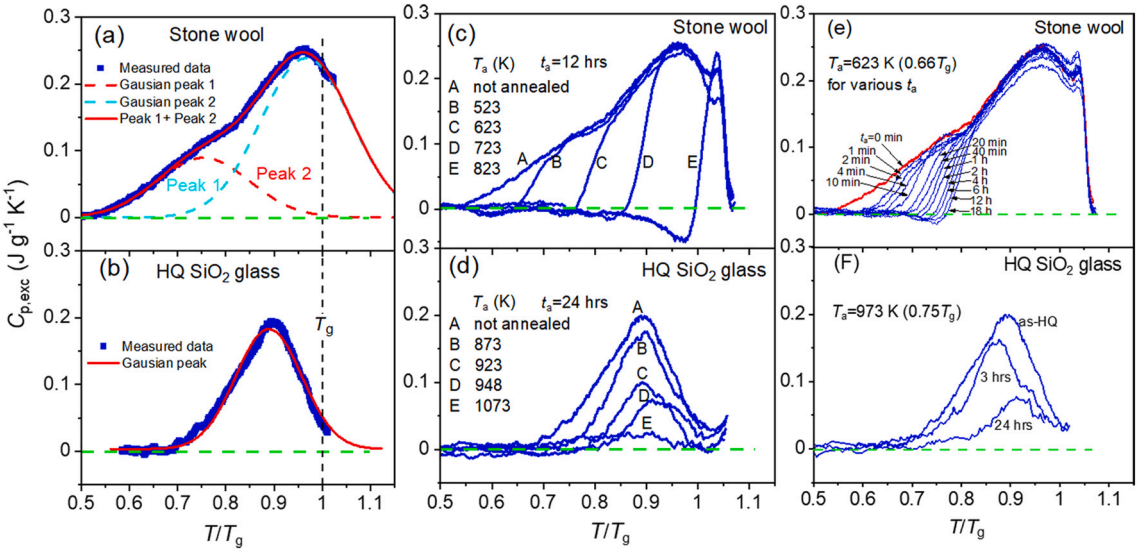

Fig. 12. Comparisons in sub-T_g relaxation between stone wool and HQ SiO_2 glass fibers before and after annealing. **(a), (b)**: The excessive heat capacity values ($C_{p,exc} = C_{p2} - C_{p1}$) as functions of the T_g normalized temperature, T/T_g (in K/K), for stone wool **(a)** and HQ SiO_2 **(b)** before annealing, respectively. The measured data are deconvoluted into the Gausian peaks. The deconvoluted curves were not reported previously. **(c), (d)**: The annealing temperature (T_a) effect on the relaxation patterns for stone wool and HQ SiO_2 glass, respectively. **(e), (f)**: The annealing time (t_a) effect. The stone wool underwent the cooling rate of about 10^6 K s^{-1}, whereas the HQ SiO_2 glass fibers were subjected to about $10^{5.5}$ K s^{-1}. All C_p values were obtained from the DSC upscans at 0.333 K s^{-1}. The deconvoluted curves in Figs. (a) and (b) were not reported previously. Figs. (a), (b), (c), (d) and (f) were reproduced with permission from [30]. Fig. (e): unpublished data.

a single megabasin, whereas a fragile system displays a proliferation of well-separated megabasins [95]. Accordingly, the two different distributions of relaxation time for stone wool are a manifestation of the diversity of deep landscape traps and of the pathways of configurational space. In contrast, the single narrow $C_{p,exc}$ peak of HQ SiO_2 should be ascribed to the less diversified depths of the potential energy minima within a megabasin compared to the relatively fragile system - stone wool.

Difference 3: Position of the energy release peak.

In Figs. 12a and b, it is seen that the departure of the $C_{p,exc}$ peak temperature from T_g for the strong system - HQ SiO_2 glass, is larger than that for the fragile system - stone wool. In other words, the $C_{p,exc}$ peak of the strong system is located at the lower T/T_g ratio than that of the strong system. The possible origin of this difference could be as follows. HQ SiO_2 glass possesses a rigid network with higher connectivity, whereas stone wool has a floppy network with lower network connectivity. Compared with the floppy network of the fragile system, the rigid network of the strong system is easier to relax via the local elastic recovery of the tetrahedral units upon heating, and thus, the relaxation occurs well below T_g. However, the floppy network undergoes not only local elastic relaxation, but also sluggish viscous relaxation, to make the latter happen, the heating temperature needs to be closer to T_g compared with the rigid network.

In addition, although slow β relaxation (JG relaxation) occurs in a strong glass-forming system [54], it largely overlaps with α relaxation. This is also why only one Gaussian fit is sufficient to cover the $C_{p,exc}$ peak, i.e., unlike the case of the fragile system stone wool, where two Gaussian functions are needed to fit the peak (Fig. 12b). Here it should be pointed out that, at same cooling rate, the T_f-T_g difference or the T_f/T_g ratio is significantly larger for a HQ strong glass system than for a HQ fragile one. This difference can be attributed to the fact that a strong glass undergoes a smaller C_p jump (ΔC_p) during glass transition than a fragile system. Consequently, a similar amount of configurational enthalpy is trapped in HQ SiO_2 glass at a much higher T_f/T_g ratio than a fragile one for the same quenching rate, when applying the enthalpy-matching method [8]. The structural rearrangement in strong liquids during cooling is more sluggish, and hence, is more readily frozen-in at a higher T_f/T_g compared with fragile ones.

Difference 4: Annealing temperature effect.

Figs. 12c and d show the difference in the influence of the annealing temperature (T_a) below T_g on the $C_{p,exc}$ peak of both the fragile system (stone wool) and the strong system (SiO_2), respectively. It is seen that, with increasing T_a, the excess potential energy of the stone wool is gradually released in the way that the onset of the $C_{p,exc}$ peak shifts to higher temperature until the peak completely vanishes when T_a approaches T_g. In contrast, the gradual release of the excess energy of HQ SiO_2 with increasing T_a takes places in the entire temperature range that the $C_{p,exc}$ peak covers, i.e., the peak height decreases until it disappears. This indicates that annealing at a single temperature (i.e., a given kinetic energy) causes the release of the excessive potential energy of the entire SiO_4 tetrahedral network. When T_a is sufficiently high, the configurationally excited structural network in HQ silica glass recovers to the structural state of the standard glass, and this is accompanied by the release of the total excess energy ($C_{p,exc}$ peak area) (Fig. 12b).

The above-mentioned differences between stone wool and HQ SiO_2 glass have two implications. First, the excess energy of a HQ fragile system is released first from thermodynamically unstable structural domains, then from less unstable ones. Second, a fragile liquid involves a larger extent of the energetic and structural heterogeneities than a strong one at comparable T/T_g.

Difference 5: Annealing time effect.

In Figs. 12e and f, $C_{p,exc}$ is plotted against T/T_g for both stone wool and HQ SiO_2 glass, to illustrate the difference in the annealing time (t_a) effect on the energy release pattern ($C_{p,exc}$ peak) between the two glass systems. Similar to the T_a effect, increasing t_a shifts $C_{p,exc}$ peak to higher temperature for stone wool (Fig. 12e), whereas it lowers the $C_{p,exc}$ peak height for HQ SiO_2 glass (Fig. 12f). This confirms again that the way of configurational sampling within PEL for strong systems differs from that for fragile ones. For a fragile system, extending t_a at a certain T_a increases the probability for some of chemical species (e.g., network modifiers) to jump from higher to lower basins in PEL, until all these species fall to the average energy level determined by T_a. During annealing in stone wool, the highly unstable structural linkages (e.g., linkages between modifier and non-bridging oxygen bonds) first relax, i.e., release their excessive energy. Finally, the 'frustrated' or 'strained' configurational states in tetrahedral SiO_4 network are fully liberated and relax towards the average energy level of the standard glass. This indicates again that the structure of fragile systems is more heterogeneous than that of strong ones. The t_a dependence of the released energy (quantified by the $C_{p,exc}$ peak area) in a fragile system is highly non-exponential.

Contrarily, the relaxation in HQ SiO_2 glass during annealing is a cooperative and collective process, during which the SiO_4 tetrahedra (short-range order) and SiO_4 tetrahedral rings (intermediate range order) collaboratively adjust themselves from their original positions to more stable ones. During this process, these structural units remain connected, and hence, relaxation of one SiO_4 unit can drive its neighboring units to relax. The cooperative relaxation is also associated with the coupled rotations of SiO_4 tetrahedra [96].

Difference 6: Shadow glass transition.

In Figs. 12c-f, we can see another pronounced difference in the way of energy release between stone wool and HQ SiO_2 glass, i.e., the shadow GT peak occurs in stone wool (see Section 3.4), but not in HQ SiO_2. The shadow GT peak of the fragile system is gradually enhanced by increasing T_a (below T_g) (Fig. 12c) or by extending t_a (Fig. 12e). Such a pre-peak is a consequence of the non-exponentiality of enthalpy relaxation, reflecting the energetic and structural heterogeneity in HQ fragile glass samples as discussed in Sections 3.3 and 3.4. The lack of the shadow GT in the strong system SiO_2 confirms its low degree of energetic and structural heterogeneities, and its lower extent of non-exponentiality of the enthalpy relaxation.

The identification of the above-mentioned 6 differences in sub-T_g relaxation behavior between a fragile and a strong glass system is important for understanding both liquid fragility [3] and PEL [9,95,97] of the glass-forming liquids. In turn, both concepts are a valuable guide for unraveling the enthalpy relaxation of both HQ glasses and annealed HQ glasses. Besides the scientific importance, the finding of these differences is also of technological importance since glass properties such as the optical and mechanical properties are strongly influenced by thermal histories (e.g., cooling rate, T_f and annealing degree), mechanical histories (e.g., tension and compression) and the repeated heating-cooling cycles [98].

3.7. *Fragile-to-strong transition, insight from 'energy bird'*

In 1999, Austen's team discovered the fragile-to-strong (F-S) transition in water, i.e., the transition of the fragile character of water in high temperature region to the strong one in the low temperature region around T_g during cooling [99]. This discovery greatly extended the liquid fragility concept and provided new insights into the glass transition and the liquid-liquid transition [3]. Later, the F-S transition was also observed in other families of glass-forming liquids such as metallic liquids [100,101], oxide liquids [102] and chalcogenide glasses [103]. The structural origins of the F—S transition and the liquid-liquid transition have been explored by conducting both experiments and atomistic simulation by several research groups [22,104,105].

Lina Hu's group observed an anomalous evolution of the 'energy bird' of numerous metallic glasses during sub-T_g annealing [106–108] and found its connection to the F-S transition [107]. In addition to these observations, they detected a non-monotonic discontinuous structure evolution with varying the sub-T_g annealing degree (temperature and time) by using the X-ray scattering technique [21,22]. Specifically, they

found that both the cluster size and the correlation length in the intermediate-range order (MRO) underwent an a three-stage change with varying the annealing temperature. The second stage corresponds to the temperature range around $1.36T_g$, where the F-S transition occurs. Based on both the structure analysis and the characteristics of the 'energy bird' of the annealed HQ CuZr(Al) glass, Zhou et al. [22] proposed a scenario of its structural evolution during the F-S transition, during which the inter-conversion between the MRO clusters with different configurations of the structural units drastically occurs as described below.

As shown in Fig. 13a, when a liquid is cooled to a certain temperature above the liquidus temperature (T_L), some of the free atoms tend to group together, leading to formation of partially symmetric icosahedra. These icosahedra continue to combine with each other to build larger clusters with a certain degree of MRO upon further cooling (Fig. 13b). During this process, the clusters in high-temperature (HT) region are partially symmetric icosahedra in a low-density state. Once the HT liquid approaches the crossing temperature between the fragile and the strong phase curves, both the number and the size of these clusters are expected to increase to a critical value, and then remain nearly constant. To minimize the system energy, these clusters must partly break down, and then are combined into more stable ones [109], i.e., those composed of fivefold-symmetric ordered icosahedra (Fig. 13c) [110,111]. When the liquid is cooled further below the crossing temperature of the F-S transition, the new stable clusters aggregate into larger ones in the high-density state at the expenses of free electrons, and then the liquid becomes a strong phase as shown in Fig. 13d. Thus, it can be stated that the interconversion between the clusters with different configurations of icosahedra is the structural origin of the F-S transition. Such interconversion was confirmed by theoretical modeling on the microstructure of CuZr(Al) liquids [112,113]. The scenario in Fig. 13 also implies that the structural heterogeneity (see Section 3.3) in the glass-forming liquids exhibiting the F-S transition evolves discontinuously with temperature. Moreover, since the F-S transition involves the disorder-order transition during cluster formation and transformation, a local exothermal process is expected to occur in a supercooled metallic glass-forming liquid during cooling. Hence, the F-S transition is a kind of the first-order transition.-

Due to the intervention of the F-S transition, the dynamics of some metallic glass-forming liquids cannot be captured by a conventional three-parameter viscosity model including the Adam-Gibbs model [114] and the Mauro-Yue-Ellison-Gupta-Allan (MYEGA) model [115]. In this regard, the MYEGA model was extended in [101] to describe the F-S transition. The details of the derivation of the extended MYEGA model are given in [101]. Compared with the original MYEGA model, the extended model includes two additional parameters that are related to the constraint onsets of two floppy-to-rigid transitions. Consequently, the size decrease of the cooperatively rearranging regions in the metallic glass-forming liquids during cooling to T_g does not follow the trend described by the Adam-Gibbs model [114], but follows the tendency reflected by the extended MYEGA model. It should be stated that both the original and the extended MYEGA models are valid in describing the viscosity-temperature relationship of glass-forming liquids under equilibrium. However, during quenching process, the decrease of the viscosity of a liquid with temperature follows a linear fashion with a significantly lower slope compared with an equilibrium liquid. The viscosity of the non-equilibrium liquid decouples from that of the equilibrium liquid at the glass transition (i.e., at T_f) during quenching. This decoupled viscosity is often called isostructural viscosity since the structure and configurational entropy remains constant during quenching [116,117]. It is also called non-equalibrium viscosity. The relationship between the non-equalibrium viscosity and temperature can be well described by the Mauro-Allan-Potuzak (MAP) model that accounts for the continuous breakdown of ergodicity at the glass transition [118].

In addition, Hu's group observed an anomalous three-steps cooling rate dependence of the activation energy of enthalpy relaxation in several HQ metallic ribbons [107]. This anomalous sub-T_g relaxation behavior was regarded as a thermodynamic signature of the F-S transition owing to the interconversion between the low and high temperature clusters in these metallic systems. Thus, it can be stated that the origin of the anomalous sub-T_g relaxation behavior is closely related to the chemical and structural heterogeneity in supercooled liquids.

4. Perspectives

There is no denying that DSC is one of the most sensitive tools to detect the potential energy fluctuation in glass, which is induced by a local structure change. As described above, the 'energy bird' approach can provide information on the potential energy landscape [9,30,97], structural heterogeneities [46,47], glass transition [9,20,58], shadow glass transition [20,24,57,79,86], fragile-to-strong transition [21,22],

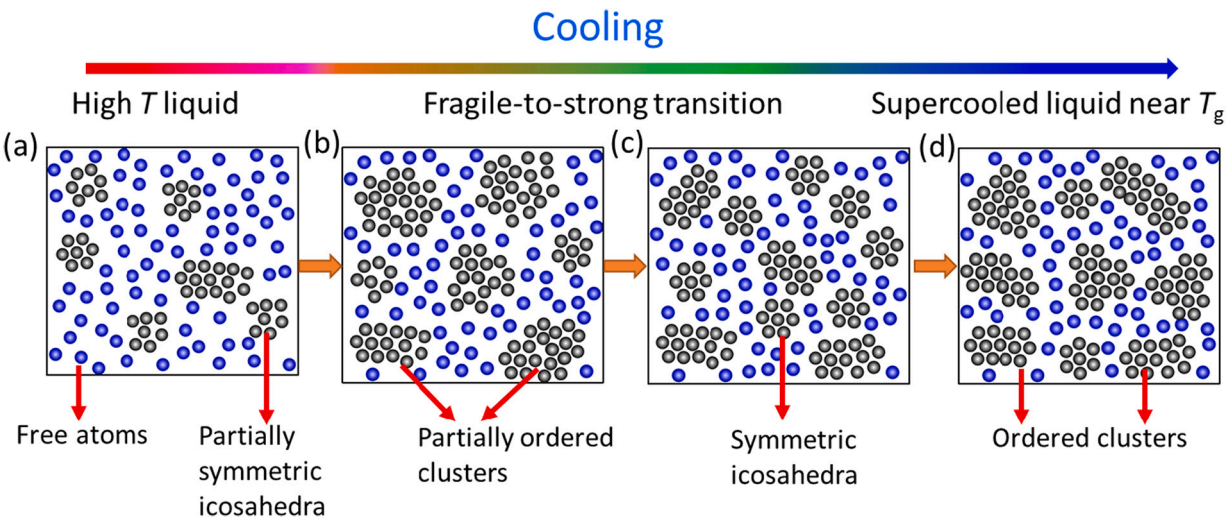

Fig. 13. Schematic of the scenario for the structural evolution in a metallic glass-forming liquid (e.g., CuZrAl system reported in [22]) during the F-S transition. **(a)** Liquid structure composed of free atoms (blue spheres) and partially ordered icosahedra (grey spheres); **(b)** Size increase of the partially ordered clusters at the beginning of the F-S transition; **(c)** Transition from partially to perfectly symmetric icosahedra; **(d)** Disorder-order transition in clusters and size increase of clusters at expense of free atoms at the ending stage of the F-—S transition above T_g. Replotted with permission from [22]. (For interpretation of the references to colour in this figure legend, the reader is referred to the web version of this article.)

secondary relaxation [53–55,79,119], and atomic vibrational dynamics [9,35] in various glass systems. The results about the sub-T_g relaxation in HQ glasses are closely related to Austen's big picture on glass and glass transition [120]. This is because the 'energy bird' approach can greatly extend the fictive temperature range of glass, and thereby a wider window of the PEL and a large structure change of glass-forming liquids can be accessed. The window of the PEL can be even significantly extended if the ultralow T_f values of ultrastable glasses [121] are combined with the T_f values of hyperquenched glasses. At the same time, it is important to develop a new technology, which could offer a quench rate close to that utilized in the molecular dynamic simulations, enabling accessing the even wider window of both PEL and the structure change in glasses and liquids. By drastically increasing the quenching rate for an oxide glass, the extremely unstable configurational states in glass will be trapped, and thereby ultrahigh T_f glasses will be obtained. Upon dynamic heating at a given rate, the ultrahigh T_f glasses will start to release their excess energy (relative to the average energy level of standard glass) at significantly lower temperature, i.e., at lower T/T_g ratios, compared with the glasses that we have investigated so far [122]. This will greatly contribute to further drawing Austen's big picture on glass and glass transition.

In addition, we should admit that both the DSC and the 'energy bird' approach alone cannot directly detect the structural heterogeneity of both glass and its supercooled liquid. In other words, the structural heterogeneity still cannot be directly visualized and quantified, and the reason for this is the lack of the characterization techniques with sufficiently high resolution to probe minor fluctuation in the intermediate range structure of glass. Thus, a quantitative link between the feature of the 'energy bird' and the structure change has not been established so far. Despite these challenges, various advanced tools for probing the local structure of glass are being rapidly developed. Importantly, new atomistic modeling approaches are emerging to predict the dynamic and thermodynamic features of glass, which the 'energy bird' approach has identified.

The rapid advance in developing new types of DSC, e.g., the flash DSC, will enable extending the window of the hyperquenching rate of supercooled liquids to glass state, thereby producing glass with extremely high fictive temperatures. In this regard, we will be able to generate the large changes in glass structure, which can be detected by advanced microscopic and spectroscopic techniques. This extended window of quenching rates will be gradually closer to the window that the future molecular dynamic simulation technique can cover. This will offer the opportunities to probe structure heterogeneities, potential energy landscape, and phase transition in 'no-man's land', i.e., in the temperature region for crystallization of supercooled liquids. The combination of the flash DSC with conventional DSC, computer modeling and structure characterization will provide insight into the structural origin of the liquid-liquid transition, the fragile-to-strong transition and the polyamorphic transition. This combination has a great potential to determine the length and time scales, at which the structural change leads to appearance of the 'energy birds' with various shapes and sizes. Moreover, if both the fictive temperature and the pressure windows are significantly widened, the understanding of the Boson peak in glass will be further deepened with the aid of advanced structural characterization techniques.

Another mission of scientists in the field of glass relaxation research is to find the connection between enthalpy relaxation features and glass properties and functionalities, which is of practical interest for developing new types of functional glasses and for improving glass performances [17,50,98,123]. Scientists will continue to reveal the nature of glass by tackling the challenging glass problems that Austen had been attempting to resolve.

Declaration of Competing Interest

The authors declare that they have no known competing financial interests or personal relationships that could have appeared to influence the work reported in this paper.

Acknowledgements

I am grateful to the late Austen Angell for his great inspiration, fruitful collaborations, and insightful advice. I thank Søren Lund Jensen, Marianne Guldberg, Mette Solvang, Dorthe Lybye, Torben Knudsen from Rockwool International for over two decades' collaborations and for providing the wonderful stone wool samples. I express my gratitude to the late Neville Greaves for fruitful collaborations, exciting discussions, and insightful advice. I thank my former co-workers studying glass relaxation: Lina Hu, Yanfei Zhang, Lasse Hornbøll, Xiaoju Guo, Min Ya, Morten Smedskjaer, Nadja Lonnroth, Chao Zhou, Qiuju Zheng, Ang Qiao and Haizheng Tao. I also thank my collaborators in investigating enthalpy relaxation in HQ glasses and mechanically deformed glasses, who are John Mauro, Prabhat Gupta, Joachim Deubener, Lothar Wondraczek, Hong Li, Marcel Potuzak, Douglas Allan, Jesper Christiansen, Li-Min Wang, John Copley, Steve Borick, Stefano Mossa, Aleksandr Chumakov, Andrea Monaco, Jiulio Monaco, Svetoslav Stankov, Haibin Yu, Maziar Montazerian, Ozgur Gulbiten, and Edgar Zanotto. I acknowledge the financial support from the Independent Research Fund Denmark and Rockwool International over the past two decades.

References

[1] C.A. Angell, Postface–a personal retrospective, in: Pascal Richet (Ed.), Encyclopedia of Glass Science, Technology, History, and Culture, Volume II, 1st edition, John Wiley and Sons, Inc., Hoboken, 2021, pp. 1457–1462.
[2] C.A. Angell, Formation of glasses from liquids and biopolymers, Science 267 (1995) 1924–1935.
[3] C.A. Angell, Liquid fragility and the glass transition in water and aqueous solutions, Chem. Rev. 102 (2002) 2627–2650.
[4] L.M. Martinez, C.A. Angell, A thermodynamic connection to the fragility of glass-forming liquids, Nature 410 (2001) 663–667.
[5] V. Velikov, S. Borick, C.A. Angell, The glass transition of water, based on hyperquenching experiments, Science 294 (2001) 2335–2338.
[6] G.P. Johari, A. Hallbrucker, E. Mayer, The glass transition of hyperquenched glassy water, Nature 330 (1987) 552–553.
[7] J. Huang, P.K. Gupta, Temperature dependence of the isostructural heat capacity of a soda lime silicate glass, J. Non-Cryst. Solids 139 (1992) 239–247.
[8] Y.Z. Yue, J.C. Christiansen, S.L. Jensen, Determination of the fictive temperature for a perquenched glass, Chem. Phys. Lett. 357 (2002) 20–24.
[9] C.A. Angell, Y.Z. Yue, L.M. Wang, J.R.D. Copley, S. Borick, S. Mossa, Potential energy, relaxation, vibrational dynamics and the boson peak, of hyperquenched glasses, J. Phys. Condens. Matter 15 (2003) S1051–S1068.
[10] A. Hasmy, S. Ispas, B. Hehlen, Percolation transitions in compressed SiO_2 glasses, Nature 599 (2021) 62–66.
[11] L. Wondraczek, S. Sen, H. Behrens, R.E. Youngman, Structure-energy map of alkali borosilicate glasses: effects of pressure and temperature, Phys. Rev. B 76 (2007), 014202.
[12] J.S. Wu, J. Deubener, J.F. Stebbins, L. Grygarova, H. Behrens, L. Wondraczek, Y. Z. Yue, Structural response of a highly viscous aluminoborosilicate melt to isotropic and anisotropic compressions, J. Chem. Phys. 131 (2009), 104504.
[13] M.M. Smedskjaer, R.E. Youngman, S. Striepe, M. Potuzak, U. Bauer, J. Deubener, H. Behrens, J.C. Mauro, Y.Z. Yue, Irreversibility of pressure induced boron speciation change in glass, Sci. Rep. 4 (2014) 3770.
[14] B. Martin, L. Wondraczek, J. Deubener, Y.Z. Yue, Mechanically induced excess enthalpy in inorganic glasses, Appl. Phys. Lett. 86 (2005), 121917.
[15] L. Hornbøll, N. Lonnroth, Y.Z. Yue, Energy release in isothermally stretched silicate glass fibers, J. Am. Ceram. Soc. 89 (2006) 70–74.
[16] M. Ya, J. Deubener, Y.Z. Yue, Enthalpy and anisotropy relaxation of glass fibers, J. Am. Ceram. Soc. 91 (2008) 745–752.
[17] M.D. Lund, Y.Z. Yue, Impact of drawing stress on the tensile strength of oxide glass fibers, J. Am. Ceram. Soc. 93 (2010) 3236–3243.
[18] M. Braun, Y.Z. Yue, C. Rüssel, C. Jäger, Two-dimensional nuclear magnetic resonance evidence for structural orientation in extruded phosphote glass, J. Non-Cryst. Solids 241 (1998) 204–207.
[19] Y.Z. Yue, S.L. Jensen, J.C. Christiansen, Physical aging in a hyperquenched glass, Appl. Phys. Lett. 81 (2002) 2983–2985.
[20] Y.Z. Yue, C.A. Angell, Clarifying the glass-transition behavior of water by comparison with hyperquenched inorganic glasses, Nature 427 (2004) 717–720.
[21] L.N. Hu, C.Z. Zhang, Y.Z. Yue, Structural evolution during the sub-T_g relaxation of hyperquenched metallic glasses, Appl. Phys. Lett. 96 (2010), 221908.
[22] C. Zhou, L.N. Hu, Q.J. Sun, H.J. Zheng, C.Z. Zhang, Y.Z. Yue, Structural evolution during fragile-to-strong transition in CuZr(Al) glass-forming liquids, J. Chem. Phys. 142 (2015), 064508.

[23] Q.J. Zheng, Y.F. Zhang, M. Montazerian, O. Gulbiten, J.C. Mauro, E.D. Zanotto, Y. Z. Yue, Understanding glass through differential scanning calorimetry, Chem. Rev. 119 (2019) 7848–7939.
[24] Y.Z. Yue, C.A. Angell, Glass transition in hyperquenched water? Reply, Nature 435 (2005) E1–E2.
[25] C.A. Angell, L.-M. Wang, S. Mossa, Y.Z. Yue, J.R.D. Copley, Vibrational dynamics and thermodynamics, ideal glass transitions and folding transitions, in liquids and in biopolymers, AIP Conf. Procs 708 (2004) 473–482.
[26] Y.Z. Yue, R. von der Ohe, S.L. Jensen, Fictive temperature, cooling rate and viscosity of glasses, J. Chem. Phys. 120 (2004) 8053–8059. Erratum: 121 (2004) 11508.
[27] D.R. Neuville, T. Charpentier, J.C. Du, Y.Z. Yue, W. Blanc, M.R. Cicconi, M. Lancry, M. Ren, Structure characterizations and molecular dynamics simulations of melt, glass, and glass fibers, in: Hong Li (Ed.), Fiberglass Science and Technology, Springer Nature Switzerland AG, 2021, pp. 89–216.
[28] Y.Z. Yue, M. Solvang, Stone and glass wool, in: Pascal Richet (Ed.), Encyclopedia of Glass Science, Technology, History, and Culture, John Wiley and Sons, Inc., Hoboken, 2021, pp. 1103–1112.
[29] Y.Z. Yue, Calorimetric studies of the structural heterogeneity of silicate liquids, Ceram. Trans. 170 (2004) 31–45.
[30] Y.Z. Yue, Anomalous enthalpy relaxation in vitreous silica, Front. Mater. 2 (2015) 54.
[31] J.D. Dana, On the composition of the capillary volcanic glass of Kilauea, Hawaii, called Pele's hair, Am. J. Sci. s3-18 [104] (1879) 134–135, https://doi.org/10.2475/ajs.s3-18.104.134.
[32] M. Potuzak, A.R.L. Nichols, D.B. Dingwell, D.A. Clague, Hyperquenched volcanic glass from Loihi seamount, Hawaii, Earth Planet. Sci. Lett. 270 (2008) 54–62.
[33] Y.Z. Yue, C. Moisescu, G. Carl, C. Rüssel, Influence of suspended iso- and anisometric crystals on the flow behaviour of fluoroapatite glass melts during extrusion, Phys. Chem. Glasses 40 (1999) 243–247.
[34] A. Qiao, T.D. Bennett, H.Z. Tao, A. Krajnc, G. Mali, C.M. Doherty, A.W. Thornton, J.C. Mauro, G.N. Greaves, Y.Z. Yue, A metal-organic framework with ultrahigh glass-forming ability, Sci. Adv. 4 (2018) eaao6827.
[35] A. Monaco, A.I. Chumakov, Y.Z. Yue, G. Monaco, L. Comez, D. Fioretto, W. A. Crichton, R. Rüffer, Density of vibrational states of a hyperquenched glass, Phys. Rev. Lett. 96 (2006), 205502.
[36] Y.Z. Yue, Hyperquenched glasses: Relaxation and properties, in: Pascal Richet (Ed.), Encyclopedia of Glass Science, Technology, History, and Culture, Volume I, 1st edition, John Wiley and Sons, Inc., Hoboken, 2021, pp. 349–358.
[37] M. Solvang, Y.Z. Yue, S.L. Jensen, D.B. Dingwell, Rheological and thermodynamic behaviors of different calcium aluminosilicate melts with the same non-bridging oxygen content, J. Non-Cryst. Solids 336 (2004) 179–188.
[38] A.Q. Tool, Relation between inelastic deformability and thermal expansion of glass in its annealing range, J. Am. Ceram. Soc. 29 (1946) 240–253.
[39] H.N. Ritland, Limitations of the fictive temperature concept, J. Am. Ceram. Soc. 39 (1956) 403–406.
[40] O.S. Narayanaswamy, A model of structural relaxation in glass, J. Am. Ceram. Soc. 54 (1971) 491–498.
[41] J.C. Mauro, R.J. Loucks, P.K. Gupta, Fictive temperature and the glassy state, J. Am. Ceram. Soc. 92 (2009) 75–86.
[42] M.A. DeBolt, A.J. Easteal, P.B. Macedo, C.T. Moynihan, Analysis of structural relaxation in glass using rate heating data, J. Am. Ceram. Soc. 59 (1976) 16–21.
[43] C.T. Moynihan, Correlation between the width of the glass transition region and the temperature dependence of the viscosity of high-T_g glasses, J. Am. Ceram. Soc. 76 (1993) 1081–1087.
[44] X.J. Guo, M. Potuzak, J.C. Mauro, D.C. Allan, T.J. Kiczenski, Y.Z. Yue, Unified approach for determining the enthalpic fictive temperature of glasses with arbitrary thermal history, J. Non-Cryst. Solids 357 (2011) 3230–3236.
[45] L. Hornbøll, Y.Z. Yue, Enthalpy relaxation in hyperquenched glasses of different fragility, J. Non-Cryst. Solids 354 (2008) 1862–1870.
[46] Y.F. Zhang, L.N. Hu, S.J. Liu, C.F. Zhu, Y.Z. Yue, Sub-T_g enthalpy relaxation in an extremely unstable oxide glass and its implication for structural heterogeneity, J. Non-Cryst. Solids 381 (2013) 23–28.
[47] Y.F. Zhang, G. Yang, Y.Z. Yue, Calorimetric signature of structural heterogeneity in a ternary silicate glass, J. Am. Ceram. Soc. 96 (2013) 3035–3037.
[48] Y.Z. Yue, Features of the relaxation in hyperquenched inorganic glasses during annealing, Phys. Chem. Glasses 46 (2005) 354–358.
[49] Y.Z. Yue, Influence of physical ageing on the excessive heat capacity of hyperquenched silicate glass fibres, J. Non-Cryst. Solids 348 (2004) 72–77.
[50] Y.F. Zhang, Y. Vulfson, Q.J. Zheng, J.W. Luo, S.H. Kim, Y.Z. Yue, Impact of fiberizing method on physical properties of glass wool fibers, J. Non-Cryst. Solids 476 (2017) 122–127.
[51] L. Wondraczek, H. Behrens, Y.Z. Yue, J. Deubener, G.W. Scherer, Relaxation and glass transition in an isostatically compressed diopside glasses, J. Am. Ceram. Soc. 90 (2007) 1556–1561.
[52] Y.Z. Yue, L. Wondraczek, H. Behrens, J. Deubener, Glass transition in an isostatically compressed calcium metaphosphate glass, J. Chem. Phys. 126 (2007), 144902.
[53] L. Hornbøll, Y.Z. Yue, Enthalpy relaxation of hyperquenched glasses and its possible link to α and β-relaxations, J. Non-Cryst. Solids 354 (2008) 350–354.
[54] L.N. Hu, Y.Z. Yue, Secondary relaxation behavior in a strong glass, J. Phys. Chem. B 112 (2008) 9053–9057.
[55] L.N. Hu, Y.Z. Yue, Secondary relaxation in metallic glass formers: its correlation with the genuine Johari-Goldstein relaxation, J. Phys. Chem. C 113 (2009) 15001–15006.
[56] G.W. Scherer, Use of the Adam-Gibbs equation in the analysis of structural relaxation, J. Am. Ceram. Soc. 67 (1984) 504–511.
[57] N. Pronina, S. Krüger, H. Bornhöft, J. Deubener, A. Ehrenberg, Cooling history of a wet-granulated blast furnace slag (GBS), J. Non-Cryst. Solids 499 (2018) 344–349.
[58] J. Pries, S. Wei, M. Wuttig, P. Lucas, Switching between crystallization from the glassy and the undercooled liquid phase in phase change material $Ge_2Sb_2Te_5$, Adv. Mater. 31 (2019) 1900784.
[59] P. Lucas, J. Pries, S. Wei, M. Wuttig, The glass transition of water, insight from phase change materials, J. Non-Cryst. Solids X 14 (2022), 100084.
[60] K. Sun, D.Z. Tan, X.Y. Fang, X.T. Xia, D.J. Lin, J. Song, Y.H. Lin, Z.J. Liu, M. Gu, Y. Z. Yue, J.R. Qiu, Three-dimensional direct lithography of stable perovskite nanocrystals in glass, Science 375 (2022) 307–310.
[61] H. Liu, W.L. Chen, R.K. Pan, Z.T. Shan, A. Qiao, J.W.E. Drewitt, L. Hennet, S. Jahn, D.P. Langstaff, H.Z. Tao, Y.Z. Yue, G.N. Greaves, From molten calcium aluminates through phase transitions to cement phases, Adv. Sci. 6 (2020) 1902209.
[62] S. Aasland, P.F. McMillan, Density-driven liquid-liquid phase-seperation in the system Al_2O_3-Y_2O_3, Nature 369 (1994) 633–636.
[63] M. Moesgaard, R. Keding, J. Skibsted, Y.Z. Yue, Evidence of intermediate-range order heterogeneity in calcium aluminosilicate glasses, Chem. Mater. 22 (2010) 4471–4483.
[64] Y.Z. Yue, Experimental evidence for the existence of an ordered structure in a silicate liquid above its liquidus temperature, J. Non-Cryst. Solids 345 (2004) 523–527.
[65] C. Zhou, M. Stepniewska, L. Longley, C.W. Ashling, P.A. Chater, D.A. Keen, T. D. Bennett, Y.Z. Yue, Thermodynamic features and enthalpy relaxation in a metal-organic framework glass, Phys. Chem. Chem. Phys. 27 (2018) 18291–18296.
[66] R. Böhmer, K.L. Ngai, C.A. Angell, D.J. Plazek, Nonexponential relaxations in strong and fragile glass formers, J. Chem. Phys. 99 (1993) 4201–4209.
[67] R.S.K. Madsen, A. Qiao, J. Sen, I. Hung, K.Z. Chen, Z.H. Gan, S. Sen, Y.Z. Yue, Ultrahigh-field 67Zn NMR reveals short-range disorder in zeolitic imidazolate framework glasses, Science 367 (2020) 1473–1476.
[68] Y.F. Zhang, P.X. Wang, T. Zheng, D.M. Li, G.D. Li, Y.Z. Yue, Enhancing Li-ion battery anode performances via disorder/order engineering, Nano Energy 49 (2018) 596–602.
[69] C.W. Gao, Z.J. Jiang, S.B. Qi, P.X. Wang, L.R. Jensen, M. Johansen, C. K. Christensen, Y.F. Zhang, D.B. Ravnsbæk, Y.Z. Yue, Metal-organic framework glass anode with an exceptional cycling-induced capacity enhancement for lithium-ion batteries, Adv. Mater. 34 (2022) 2110048.
[70] H. Tong, H. Tanaka, Structural order as a genuine control parameter of dynamics in simple glass formers, Nat. Commun. 10 (2019) 5596.
[71] G. Jug, A. Loidl, H. Tanaka, On the structural heterogeneity of supercooled liquids and glasses (a), Europhys. Lett. 133 (2021) 56002.
[72] G.P. Johari, Water's T_g-endotherm, sub-T_g peak of glasses and T_g of water, J. Chem. Phys. 119 (2003) 2935–2937.
[73] G.P. Johari, Calorimetric features of high-enthalpy amorphous solids and glass-softening temperature of water, J. Phys. Chem. 107 (2003) 9063–9070.
[74] I. Kohl, L. Bachmann, E. Mayer, A. Hallbrucker, T. Loerting, Glass transition in hyperquenched water? Nature 435 (2005) E1.
[75] N. Giovambattista, C.A. Angell, F. Sciortino, H.E. Stanley, Glass-transition temperature of water: a simulation study, Phys. Rev. Lett. 93 (2004), 047801.
[76] J. Swenson, H. Jansson, R. Bergman, Relaxation processes in supercooled confined water and implications for protein dynamics, Phys. Rev. Lett. 96 (2006), 247802.
[77] S. Capaccioli, K.L. Ngai, Resolving the controversy on the glass transition temperature of water? J. Chem. Phys. 135 (2011), 104504.
[78] J.J. Shephard, C.G. Salzmann, Molecular reorientation dynamics govern the glass transitions of the amorphous ices, J. Phys. Chem. Lett. 7 (2016) 2281–2285.
[79] Q. Yang, S.X. Peng, Z. Wang, H.B. Yu, Shadow glass transition as a thermodynamic signature of β relaxation in hyper-quenched metallic glasses, Natl. Sci. Rev. 7 (2020) 1896–1905.
[80] H.S. Chen, A. Inoue, Sub-T_g enthalpy relaxation in PdNiSi alloy glasses, J. Non-Cryst. Solids 61&62 (1984) 805–810.
[81] A.R. Berens, I.M. Hodge, Effects of annealing and prior history on enthalpy relaxation in glassy polymers. 1. Experimental study on poly (vinyl chloride), Macromolecules 15 (1982) 756–761.
[82] O. Gulbiten, J.C. Mauro, P. Lucas, Relaxation of enthalpy fluctuations during sub-T_g annealing of glassy selenium, J. Chem. Phys. 138 (2013), 244504.
[83] L. Hornbøll, T. Knudsen, Y.Z. Yue, X.J. Guo, Heterogeneous enthalpy relaxation in glasses far from equilibrium, Chem. Phys. Lett. 494 (2010) 37–40.
[84] J. Deubener, Y.Z. Yue, H. Bornhöft, M. Ya, Decoupling between birefringence decay, enthalpy relaxation and viscous flow in calcium boroalumosilicate glasses, Chem. Geol. 256 (2008) 298–304.
[85] C. Hermansen, J.C. Mauro, Y.Z. Yue, A model for phosphate glass topology considering the modifying ion sub-network, J. Chem. Phys. 140 (2014), 154501.
[86] Y.Z. Yue, 'Shadow' glass transition in glass, Natl, Sci. Rev. 8 (2021) nwab160.
[87] Q. Yang, C.Q. Pei, H.B. Yu, T. Feng, Metallic nanoglasses with promoted β-relaxation and tensile plasticity, Nano Lett. 21 (2021) 6051–6056.
[88] G.P. Johari, M. Goldstein, Viscous liquids and the glass transition. II. Secondary relaxations in glasses of rigid molecules, J. Chem. Phys. 53 (1970) 2372–2388.
[89] K.L. Ngai, S. Capaccioli, Relation between the activation energy of the Johari-Goldstein β relaxation and T_g of glass formers, Phys. Rev. E 69 (2004), 031501.

[90] J.A. Kalb, M. Wuttig, F. Spaepen, Calorimetric measurements of structural relaxation and glass transition temperatures in sputtered films of amorphous Te alloys used for phase change recording, J. Mater. Res. 22 (2007) 748.
[91] A.I. Chumakov, G. Monaco, A. Fontana, A. Bosak, R. Hermann, D. Bessas, B. Wehinger, W.A. Crichton, M. Krisch, R. Rüffer, G. Baldi, G. Carini, G. D'Angelo, E. Gilliioli, G. Tripodo, M. Zanatta, B. Winkler, V. Milman, K. Refson, M. Tucker, L. Dubrovinsky, R. Keding, Y.Z. Yue, Role of disorder in the thermodynamics and atomic dynamics of glasses, Phys. Rev. Lett. 112 (2014), 025502.
[92] H. Shintani, H. Tanaka, Universal link between the boson peak and transverse phonons in glass, Nat. Mater. 7 (2008) 870–877.
[93] T.S. Grigera, V. Martin-Mayor, G. Parisi, P. Verrocchio, Phonon interpretation of the 'boson peak' in supercooled liquids, Nature 422 (2003) 289–292.
[94] C.A. Angell, Spectroscopy simulation and scattering, and the medium range order problem in glass, J. Non-Cryst. Solids 73 (1985) 1–17.
[95] P.G. Debenedetti, F.H. Stillinger, Supercooled liquids and the glass transition, Nature 410 (2001) 259–267.
[96] U. Buchenau, N. Nücker, A.J. Dianoux, Neutron scattering study of the low-frequency vibrations in vitreous silica, Phys. Rev. Lett. 53 (1984) 2316.
[97] M. Goldstein, Viscous liquids and the glass transition: a potential energy barrier picture, J. Chem. Phys. 51 (1969) 3728–3739.
[98] S.V. Ketov, Y.H. Sun, S. Nachum, Z. Lu, A. Checchi, A.R. Beraldin, H.Y. Bai, W. H. Wang, D.V. Louzguineluzgin, M.A. Carpenter, A.L. Greer, Rejuvenation of metallic glasses by non-affine thermal strain, Nature 524 (2015) 200–203.
[99] K. Ito, C.T. Moynihan, C.A. Angell, Thermodynamic determination of fragility in liquids and a fragile-to-strong liquid transition in water, Nature 398 (1999) 492–495.
[100] C. Way, P. Wadhwa, R. Busch, The influence of shear rate and temperature on the viscosity and fragility of the $Zr_{41.2}Ti_{13.8}Cu_{12.5}$ $Ni_{10.0}Be_{22.5}$ metallic-glass-forming liquid, Acta Mater. 55 (2007) 2977.
[101] C.Z. Zhang, L.N. Hu, Y.Z. Yue, J.C. Mauro, Fragile-to-strong transition in metallic glass-forming liquids, J. Chem. Phys. 133 (2010), 014508.
[102] H. Liu, W.L. Chen, R.K. Pan, Z.T. Shan, A. Qiao, J.W.E. Drewitt, L. Hennet, S. Jahn, D.P. Langstaff, H.Z. Tao, Y.Z. Yue, G.N. Greaves, From molten calcium aluminates through phase transitions to cement phases, Adv. Sci. 6 (2020) 1902209.
[103] P. Lucas, Fragile-to-strong transitions in glass forming liquids, J. Non-Cryst. Solids 557 (2021), 119367.
[104] H. Tanaka, Liquid–liquid transition and polyamorphism, J. Chem. Phys. 153 (2020), 130901.
[105] W. Chu, J. Shang, K. Yin, N. Ren, L. Hu, Y. Zhao, B. Dong, Generality of abnormal viscosity drop on cooling of CuZr alloy melts and its structural origin, Acta Mater. 196 (2020) 690–703.
[106] L.N. Hu, Y.Z. Yue, C.Z. Zhang, Abnormal sub-T_g enthalpy relaxation in the CuZrAl metallic glasses far from equilibrium, Appl. Phys. Lett. 98 (2011), 081904.
[107] L.N. Hu, C. Zhou, C.Z. Zhang, Y.Z. Yue, Thermodynamic anomaly of the sub-T_g relaxation in hyperquenched metallic glasses, J. Chem. Phys. 138 (2013), 174508.
[108] C. Wang, L.N. Hu, C. Wei, X. Tong, C. Zhou, Q. Sun, X. Hui, Y.Z. Yue, Sub-T_g relaxation patterns in cu-based metallic glasses far from equilibrium, J. Chem. Phys. 141 (2014), 164507.
[109] W. Yang, J. Li, H. Liu, C. Dun, H. Zhang, J. Huo, L. Xue, Y. Zhao, B. Shen, L. Dou, A. Inoue, Origin of abnormal glass transition behavior in metallic glasses, Intermetallics 49 (2014) 52.
[110] X.D. Wang, Q.K. Jiang, Q.P. Cao, J. Bednarcik, H. Franz, J.Z. Jiang, Atomic structure and glass forming ability of Cu46Zr46Al8 bulk metallic glass, J. Appl. Phys. 104 (2008), 093519.
[111] H.Z. Fang, X. Hui, G.L. Chen, Z.K. Liu, Al-centered icosahedral ordering in bulk metallic glass, Appl. Phys. Lett. 94 (2009), 091904.
[112] V. Wessels, A.K. Gangopadhyay, K.K. Sahu, R.W. Hyers, S.M. Canepari, J. R. Rogers, M.J. Kramer, A.I. Goldman, D. Robinson, J.W. Lee, J.R. Morris, K. F. Kelton, Rapid chemical and topological ordering in supercooled liquid $Cu_{46}Zr_{54}$, Phys. Rev. B 83 (2011), 094116.
[113] A. Hirata, L.J. Kang, T. Fujita, B. Klumov, K. Matsue, M. Kotani, A.R. Yavari, M. W. Chen, Geometric frustration of icosahedron in metallic glasses, Science 341 (2013) 376.
[114] G. Adam, J.H. Gibbs, On the temperature dependence of cooperative relaxation properties in glass-forming liquids, J. Chem. Phys. 43 (1965) 139–146.
[115] J.C. Mauro, Y.Z. Yue, A.J. Ellison, P.K. Gupta, D.C. Allan, Viscosity of glass-forming liquids, Proc. Natl. Acad. Sci. U. S. A. 106 (2009) 19780–19784.
[116] O.V. Mazurin, Y.K. Startsev, S.V. Stoljar, Temperature dependences of viscosity of glass-forming substances at constant fictive temperatures, J. Non-Cryst. Solids 52 (1982) 105–114.
[117] Y.Z. Yue, The iso-structural viscosity, configurational entropy and fragility of oxide liquids, J. Non-Cryst. Solids 355 (2009) 737–744.
[118] J.C. Mauro, D.C. Allan, M. Potuzak, Nonequilibrium viscosity of glass, Phys. Rev. B 80 (2009), 094204.
[119] A. Qiao, P. Wang, H.Z. Tao, Y.Z. Yue, Sub-T_g enthalpy relaxation in milled and quenched As_2S_3 glasses, J. Non-Cryst. Solids 500 (2018) 225–230.
[120] C.A. Angell, K.L. Ngai, G.B. McKenna, P.F. McMillan, S.W. Martin, Relaxation in glassforming liquids and amorphous solids, J. Appl. Phys. 88 (2000) 3113–3157.
[121] S.F. Swallen, K.L. Kearns, M.K. Mapes, Y.S. Kim, R.J. McMahon, M.D. Ediger, T. Wu, L. Yu, S. Satija, Organic glasses with exceptional thermodynamic and kinetic stability, Science 315 (2007) 353–356.
[122] Y.Z. Yue, Characteristic temperatures of enthalpy relaxation in glass, J. Non-Cryst. Solids 354 (2008) 1112–1118.
[123] N. Lonnroth, C.L. Muhlstein, C. Pantano, Y.Z. Yue, Nanoindentation of glass wool fibers, J. Non-Cryst. Solids 354 (2008) 3887–3895.